Examining the provenance of branched GDGTs in the Tagus River drainage basin and its outflow in the Atlantic Ocean over the Holocene to determine their usefulness for paleoclimate applications

Lisa Warden[a], *Jung-Hyun Kim*[a,b], *Claudia Zell*[a,c], *Geert-Jan Vis*[d], *Henko de Stigter*[e], *Jérôme Bonnin*[f], *and Jaap S. Sinninghe Damsté*[a,g]

[a]*NIOZ Netherlands Institute for Sea Research, Department of Marine Microbiology and Biogeochemistry, and Utrecht University, P.O. Box 59, 1790 AB Den Burg, the Netherlands*

[b]Present address: *Korea Polar Research Institute, 26 Songdomirae-ro, Yeonsu-gu, Incheon 21990, South Korea*

[c]Present address: *Pierre and Marie Curie University - Paris 6 · METIS - UMR 7619 France*

[d]*TNO, Geological Survey of the Netherlands, P.O. Box 80015, 3508 TA Utrecht, the Netherlands*

[e]*NIOZ Netherlands Institute for Sea Research, Department of Ocean Systems Sciences, and Utrecht University, PO Box 59, 1790 AB Den Burg, the Netherlands*

[f]*UMR-EPOC 5805 CNRS, Université de Bordeaux, Allée Geoffroy St Hilaire, 33615 Pessac, France*

[g]*Utrecht University, Faculty of Geosciences, Department of Earth Sciences, PO Box 80021, 3508 TA Utrecht, the Netherlands*

Correspondence to: Lisa Warden (lisa.warden@nioz.nl)

Keywords: Tagus River basin, Holocene, temperature reconstructions, branched glycerol dialkyl glycerol tetraethers, paleoclimate

Abstract

The distributions of branched glycerol dialkyl glycerol tetraethers (brGDGTs), which are transported from the soils where they are predominantly produced to marine sediments via rivers, have been applied in reconstructing mean annual air temperatures (MAT) and pH of soils. However, paleoclimate reconstructions using sedimentary brGDGTs have proven difficult in arid regions including the Iberian Peninsula. Recently, six novel 6-methyl brGDGTs have been described using new analytical methods (in addition to the nine 5-methyl brGDGTs previously used for climate reconstructions), and so new pH and MAT calibrations have been developed that in a set of global soil samples were shown to improve the accuracy of reconstructions, especially in arid regions. Because of this we decided to apply the new method to separate the 5- and 6-methyl isomers along with the novel calibrations to a sample set that runs in a transect from source to sink along the Tagus River and out to the deep ocean off the Portuguese margin and spans the last 6,000 years in order to determine if it improves paleoclimate reconstructions in this area. We found that although pH reconstructions in the soils were improved using the new calibration, MAT reconstructions were not much better even with the separation of the 5- and 6-methyl brGDGTs. This confirmed the conclusion of previous studies that the amount of aquatically produced brGDGTs is overwhelming the soil derived ones in marine sediments and complicating MAT reconstructions in the region. Additionally, the new separation revealed a strong relationship between the new degree of cyclization (DC') of the brGDGTs and MAT not seen before that could be making temperature reconstructions in this and other arid regions difficult.

1. Introduction

Understanding past climate variability is important for predicting future climate change as well as how ecosystems, organisms and human society could be affected. The validation of climate proxies is imperative for the correct interpretation of climate archives and therefore also for the climate models building on these past climate data. Terrestrial environments play an important role in global climate, however, continental climate reconstructions are hindered by the lack of continental temperature proxies. In the future, changes in terrestrial climate are likely to have a large impact on human society just as they had in the past (e.g. Haug et al., 2003). Availability of trustworthy temperature data from the terrestrial environment will be essential for the development of reliable climate models.

The distribution of branched glycerol dialkyl glycerol tetraethers (brGDGTs, Fig. S1), a group of membrane-spanning lipids that occur in heterotrophic bacteria (Pancost and Sinninghe Damsté, 2003; Weijers et al., 2010) pervasive in peat (Weijers et al., 2006) and worldwide in soils has proven useful as a tool to obtain high resolution, continental temperature reconstructions (Weijers et al., 2007a; Schouten et al., 2008; Bendle et al., 2010). BrGDGTs are biosynthesized by bacteria (Sinninghe Damsté et al., 2011; 2014) living in soils and the distribution of brGDGTs in soils is affected by growth temperature and pH (Weijers et al., 2006). More specifically, the degree of methylation of the brGDGTs (expressed as methylation of branched tetraethers index, MBT; see Table S1 for a detailed explanation of all GDGT indices used in this study) relates to mean annual air temperature (MAT), and to a lesser extent soil pH, whereas the degree of cyclization (DC) of the brGDGTs (also expressed as the cyclization of branched tetraethers index, CBT) correlates solely with soil pH (Weijers et al., 2007a). MBT has recently been amended to become MBT' by eliminating the brGDGTs that rarely occur in soils (Peterse et al., 2012). These observations led to the development of a continental paleoclimate proxy based on the distribution of brGDGTs that

has been applied in paleosoils (Peterse et al., 2009; Weijers et al., 2007a; 2011). Branched GDGTs that are produced in soils are washed by runoff into streams and rivers where they are transported to and deposited in river sediment and in coastal marine sediment that are under the influence of major river systems. In this way, brGDGTs have been used as recorders of the continental paleoclimate (Weijers et al., 2007b; Bendle et al., 2010; Hren et al., 2010; Keating-Bitonti et al., 2011).

Complications using brGDGTs as a proxy for MAT have arisen in some settings. In marine sediments receiving a low input of soil organic matter (OM), it was found that the distribution of brGDGTs and the reconstructed temperatures were quite different from that observed in regional soils (Peterse et al., 2009). Peterse et al. (2012) found in arid regions temperature is no longer an important control on the distribution of brGDGTs and therefore MAT reconstructions in these areas should be interpreted with care. In the Iberian Peninsula, Menges et al. (2014) found that MBT' was not correlated to MAT but instead correlated with the aridity index (AI), a parameter for water availability in soils, and mean annual precipitation (MAP). In drainage basins with varying soil sources that had different MATs (i.e. mountainous vs. lowland), it was found that the provenance of the soil matter must be considered when interpreting MAT reconstructions (Bendle et al., 2010). In-situ production of brGDGTs can occur within the river systems (Yang et al., 2012; Zell et al., 2013, De Jonge et al., 2014b) and cause brGDGT distributions and MAT reconstructions that differ from those in the soils of the source area. These complications make it vital to investigate how varying environmental conditions, the transport of these terrestrially derived fossilized lipids, and in-situ production affect the implementation of brGDGTs for paleoclimate reconstructions.

Recently a set of six new brGDGT isomers that differ in the position of the methyl groups were identified and described (De Jonge et al., 2013). The relative abundance of these novel, 6-methyl brGDGTs are strongly dependent on pH and so by excluding them from the

MBT' index (newly defined as MBT'_{5ME}) the correlation with MAT is improved (De Jonge et al., 2014a). The CBT index was also redefined in this study, as CBT', to include all of the pH dependent 6-methyl brGDGTs and consequently yielded a higher correlation with soil pH as a result (De Jonge et al., 2014a). De Jonge et al. (2014a) also developed, based on a dataset of globally distributed soils, a new pH calibration taking into account the new CBT' as well as new MAT calibrations, defined as MAT_{mr} and MAT_{mrs}. In a global soil set they were shown to improve the accuracy of reconstructions, especially in arid regions. These indices and calibrations were applied in a coastal sediment core in the Northern Kara Sea off Siberia in a study emphasizing the importance of examining the provenance of brGDGTs when using these lipids for paleoclimate reconstructions (De Jonge et al., 2015).

A comprehensive study has been previously performed on the present day transport of brGDGTs in the Tagus River basin from source to sink (Zell et al., 2014). The results from this study demonstrated that the distribution of brGDGTs in the riverine suspended particulate matter (SPM) did not reflect that of the soils, implying that due to the aquatic production in river and marine environments the use of brGDGTs for paleoclimate reconstructions in the region would be complicated (Zell et al., 2014; 2015). Here we examine if the assessment of the provenance of brGDGTs in the Tagus River basin can be improved by the application of the analytical methods allowing the separation of the 5- and 6-methyl brGDGTs (De Jonge et al., 2013). In addition, we examine if the provenance of brGDGTs changed over the Holocene and if the distribution of brGDGTs in the past reflected continental sources and thus past temperature and pH of the soils in the drainage basin of the river. To this end we compare the down core brGDGT distributions in Holocene sediments retrieved from four locations along a transect in the Tagus River basin, which includes the river floodplain (Tagus River Floodplain core), the offshore mudbelt (Mudbelt core), and marine sediments from the canyons (Lisbon Canyon Head core and Lower-Sétubal canyon core) (Fig. 1), and compare them to brGDGT

126 distributions of soil and river SPM from the Tagus River watershed. This allows insight into
127 the potential and limitations of using the novel MAT_{mrs}/CBT' proxies for climate
128 reconstruction in this region and in river systems in general.
129
130 **1.1 Study Area**
131 The Tagus River drains the central part of the Spanish Plateau with an E-W orientation
132 (Benito et al., 2003). The waters originate at an elevation of about 1600 m altitude in eastern
133 Spain at the Iberian Range and the mouth of the river feeds into the Atlantic Ocean near
134 Lisbon (Vis and Kasse, 2009). At 1,200 km long the Tagus River is the longest river of the
135 Iberian Peninsula and it occupies 82×10^3 km^2 making it the third largest in catchment area
136 (Benito et al., 2003). The Tagus Basin is surrounded by mountains on three sides with the
137 Iberian Range to the east, the Central Range to the north, and the Toledo Mountains to the
138 south. Present-day mean discharge at the Tagus River mouth is 400 m^3 s^{-1} (Vale and Catarino,
139 1996; Vaz et al., 2011) and the largest contribution of draining tributaries comes from the
140 Central Range in the North (Benito et al., 2003). The Tagus River is characterized by extreme
141 seasonal and annual variability, including periods of flooding with 30 times the mean
142 discharge and an annual discharge cycle characterized by two peaks in the winter (December
143 and then again February to March) and a discharge minimum in the summer (August) (Benito
144 et al., 2003). Since the 1940s dams have been built along the expanse of the Tagus River for
145 water supply, hydropower, and flood prevention (Dias et al., 2002), which have likely
146 impacted the transport of brGDGTs in the Tagus River system since their construction.
147 Where the Tagus River debouches into the Atlantic Ocean, the narrow continental shelf
148 and steep continental slope are deeply incised by the Lisbon-Setúbal canyon system. The head
149 of the Lisbon branch of that canyon system is located 13 km offshore from the Tagus River
150 mouth at 120 m water depth. From that point, the canyon descends over a length of 165 km

151 until it opens out onto the Tagus Abyssal Plain at 4860 m (Lastras et al., 2009). Even though
152 the shelf is very narrow, sparse amounts of continental organic matter and clastic sediment
153 reach the deep ocean in this region (Jouanneau et al., 1998; de Stigter et al., 2011; Vis et al.,
154 in press). This is because the Lisbon-Setúbal canyon is not a very dynamic system and has a
155 weak down-canyon transport of sediments (Jouanneau et al., 1998; Jesus et al., 2010; de
156 Stigter et al., 2011). A part of the continental shelf in this region is covered by mud deposits,
157 which originate predominantly from the Tagus estuary (Jouanneau et al., 1998). According to
158 this same study, the mouth of the much smaller Sado River is located further to the southeast
159 and contributes only a relatively minor sediments volume to the shelf mud deposits.

160 Generally, the climate of the Tagus River Basin is characterized by seasonal variability
161 and is considered continental Mediterranean (Le Pera and Arribas, 2004). Summers in the
162 Tagus region are hot and dry and the winters are relatively mild and wet (Benito et al., 2003).
163 During the summers, the climate regime in the Tagus Basin is controlled by the Azores high
164 and in the winter by the westerlies (Benito et al., 2003). The MAT in the interior regions of
165 the Tagus River basin varies from the highlands to the lowlands of the inner basin from 7.5 to
166 12.5°C, respectively and can increase up to 16°C along the Atlantic Coast (Le Pera and
167 Arribas, 2004). The mean annual precipitation in the lowlands of the inner basin is mostly
168 below 500 mm making it an arid region, however, some of the highest altitudes of the
169 mountainous areas have a larger mean annual precipitation ranging from 750-1200 mm (Le
170 Pera and Arribas, 2004).

171 The Iberian Peninsula is located between two major pressure systems, the Azores High
172 and the Iceland Low, which make up the North Atlantic Oscillation (NAO). This climate
173 phenomenon is caused by the varying pressure gradient in the North Atlantic and greatly
174 influences climate conditions all over Europe (Hurrell, 1995; Hurrell and VanLoon, 1997).
175 Because of the Iberian Peninsula's advantageous position for studying the shifting NAO, the

176 climate in this region has been intensively investigated (Zorita et al., 1992; Rodó et al., 1997;
177 Trigo et al., 2004). Many of these studies are from an oceanic perspective, obtaining sea
178 surface temperatures from marine sediments using the alkenone unsaturation indices
179 (Abrantes et al., 2005, 2009; Rodrigues et al., 2009), coccolithophore assemblages (Cachao
180 and Moita, 2000; Palumbo et al., 2013), and stable isotopic oxygen composition of
181 foraminifera (Lebreiro et al., 2006 ; Bartels-Jónsdóttir et al., 2006; 2009). The terrestrial
182 climate has been examined using continental paleoarchives such as speleothems (Munoz-
183 Garcia et al., 2007; Martin-Chivelet et al., 2011; Stoll et al., 2013), tree rings (Andreu et al.,
184 2007; Linan et al., 2012), and pollen (Huntley and Prentice, 1988; Lebreiro et al., 2006; Davis
185 et al., 2003; Fletcher et al., 2007; Corella et al., 2013). The integrated continental and marine
186 approach can give complimentary information to past climate in a region and by using the
187 same proxy on the continent, in the ocean, and at the ocean-continent interface we would
188 perhaps obtain a clearer picture of continental climate processes in an area rather than using
189 separate studies or a multi-proxy approach.
190

191 ## 2. Material and Methods

192 **Sample collection**. Soil samples, riverbank sediment samples, and river SPM from the Tagus
193 River basin (Fig. 1b) were collected previously (Zell et al., 2014). These samples were
194 complemented with four long sediment cores collected along a transect running from the
195 Tagus River to the lower continental slope (Fig. 1). The Tagus River Floodplain core
196 (0501.029) was collected in a low-energy backswamp of the present-day floodplain of the river
197 at ~4 km west of the Tagus channel (Table 1). The sediment was collected using an Edelman
198 hand auger for sediment above the groundwater table and a gauge for sediment below the
199 groundwater table (Vis et al., 2008). The sediments were wrapped in the field for laboratory
200 analyses. The other three cores were collected using a piston corer, during campaigns in May

2007 and March 2011 with RV *Pelagia* conducted by the NIOZ - Royal Netherlands Institute for Sea Research. The coring site for the Mudbelt core (64PE332-30-2) was to the west of the Tagus Estuary mouth, for the Lisbon Canyon Head core (64PE332-44-2) it was to the east of the Tagus Estuary mouth, and for the Lower Setúbal Canyon core (64PE269-39) it was on the crest of the northern levee of the lower Setúbal Canyon (Table 1). A detailed description of the cores used in this study is given in the Supplemental Information.

Age models. The accelerated mass spectrometry (AMS) ^{14}C measurements of the three marine sediment cores were carried out at the BETA analytic laboratory (USA) on benthic or planktonic forams, gastropods or shells fragments (Table 2). As for the Tagus River Floodplain core, the radiocarbon dating material was performed for a previous study and consisted of mostly terrestrial botanical macrofossils, but other bulk material was used as well (Vis et al., 2008). In order to establish consistent chronologies for the four sediment cores, all the AMS dates were calibrated into calendar ages using the CALIB 7.0, available at http://radiocarbon.pa.qub.ac.uk/calib (Stuiver et al., 1998). The calibration data and curve selection used for the three marine sediment cores was Marine13 and for the Tagus River Floodplain core IntCal13 was used (Reimer et al., 2013). All radiocarbon dates mentioned have age spans at the 2σ range and are expressed as calibrated ages (cal. BP) (Table 2, Fig. S2).

Bulk isotope data Prior to bulk carbon isotope analysis, sediment was decalcified using a 2 N HCL solution for approximately 18 h. The sediment was rinsed three times using double-distilled water and then freeze dried again. Total organic carbon (TOC) and $\delta^{13}C_{TOC}$ (Table 3) were measured in duplicate using the Flash 2000 series Organic Elemental Analyzer (Thermo

225 Scientific) equipped with a TCD detector. The $\delta^{13}C_{TOC}$ is expressed in relation to the Vienna
226 PeeDee Belemnite (VPDB) standard and the isotope analysis precision was 0.1‰.

227

228 **Lipid extraction and GDGT analysis.** Between 1-3 g of freeze dried sediment was extracted
229 using the Dionex™ accelerated solvent extraction (ASE) with dilchloromethane
230 (DCM):methanol (9:1, v/v) as the solvent at a temperature of 100°C and a pressure of 1500
231 psi for 5 min with 60 % flush and purge 60 seconds. The extract was then collected and dried
232 using Caliper Turbovap®LV. Next, using DCM, the lipid extract was dried over a column of
233 anhydrous Na_2SO_4 and then blown down under a gentle stream of N_2. In order to quantify
234 GDGTs, 1 µg of an internal standard (C_{46} GDGT; Huguet et al., 2006) was added to the total
235 lipid extract before it was separated over a column of Al_2O_3 (activated for 2 h at 150°C) into
236 three fractions using hexane:DCM (9:1, v:v) for the apolar fraction, hexane:DCM (1:1, v:v)
237 for the ketone fraction and DCM:MeOH (1:1, v:v) for the polar fraction. The polar fraction,
238 which contained the GDGTs, was dried under a N_2 stream and then re-dissolved in
239 hexane:isopropoanol (99:1, v:v) at a concentration 10 mg ml^{-1}. Finally it was passed through a
240 0.45 µm PTFE filter and analysed with high performance liquid chromatography-atmospheric
241 pressure positive ion chemical ionization–mass spectrometry (HPLC-APCI-MS) with a
242 separation method that allows the separation of 5- and 6-methyl brGDGTs (Hopmans et al.,
243 2015). For the study of Zell et al., (2014) the samples were split into two different fractions
244 before the analysis, the intact polar lipid (IPL) fraction and core lipid (CL) fractions. For the
245 purposes of this study the IPL and CL fractions of the river SPM were analyzed separately on
246 the HPLC-APCI-MS for GDGTs (Hopmans et al., 2015) and then the amount of GDGTs
247 found in the CL and IPL fractions were combined. After analysis some of the GDGT based
248 indices were recalculated for the entire sample set.

Calculation of GDGT-based proxies. The Roman numerals refer to the GDGTs indicated in Fig. S1. The 5-methyl brGDGTs and 6-methyl brGDGTs are distinguished by an accent on the 6-methyl brGDGTs. The GDGT indicated by IV is crenarchaeol, the isoprenoid GDGT specific to Thaumarchaeota (Sinninghe Damsté et al., 2002).

The BIT index (Hopmans et al., 2003), which results in a value between 0 and 1 with those values closer to 0 designating a more marine signal and a value close to 1 indicating a more terrestrial signal, was calculated using the following formulae that specifically includes the novel 6-methyl brGDGTs according to De Jonge et al. (2015):

$$\text{BIT index} = (Ia+IIa+IIIa+IIa'+IIIa')/(Ia+IIa+IIIa+IIa'+IIIa'+IV) \quad (1)$$

The isomer ratio (IR) signifies the quantity of the penta- and hexamethylated 6-Me brGDGTs compared to the total brGDGTs and was calculated according to De Jonge et al., (2015):

$$IR=(IIa'+IIb'+IIc'+IIIa'+IIIb'+IIIc')/(IIa+IIb+IIc+IIIa+IIIb+IIIc+IIa'+IIb'+IIc'+IIIa'+IIIb'+IIIc') \quad (2)$$

The relative abundance of the penta- and hexamethylated 6-methyl brGDGTs are calculated according to (De Jonge et al., 2014b):

$$IR_{II} = IIa'/(IIa+IIa') \quad (3)$$

$$IR_{III} = IIIa'/(IIIa+IIIa') \quad (4)$$

The MBT'_{5Me} (which excludes the 6-methyl brGDGTs) was used to calculate MAT according to De Jonge et al., (2014a):

$$MBT'_{5Me} = (Ia+Ib+Ic)/(Ia+Ib+Ic+IIa+IIb+IIc+IIIa) \quad (5)$$

$$MAT = -8.57 + 31.45 * MBT'_{5Me} \quad (6)$$

The equation to determine DC (Sinninghe Damsté et al., 2009) was reformulated to specifically include the pentamethylated 6-methyl brGDGTs:

$$DC' = (Ib+IIb+IIb')/(Ia+Ib+IIa+IIb+IIa'+IIb') \quad (7)$$

To calculate pH and MAT the novel MAT_{mr} /CBT' calibration was used (De Jonge et al., 2014a):

$$CBT' = {}^{10}\log[(Ic+IIa'+IIb'+IIc'+IIIa'+IIIb'+IIIc')/(Ia+IIa+IIIa)] \quad (8)$$

$$pH = 7.15 + 1.59 * CBT' \quad (9)$$

$$MAT_{mr} = 7.17 + 17.1 * [Ia] + 25.9 * [Ib] + 34.4 * [Ic] - 28.6 * [IIa] \quad (10)$$

$$MAT_{mrs} = 5.58 + 17.91 * [Ia] - 18.77 * [IIa] \quad (11)$$

Statistical analysis. Using R software package for statistical analysis we employed principal component analysis (PCA) based on the correlation matrix. The PCA was performed on the fractional abundances of all 15 of the 5- and 6-methyl brGDGTs for the entire sample set along the transect from the land to the ocean.

3. Results

We report bulk and brGDGT data for four cores covering Holocene sedimentation in the Tagus River Basin and its outflow into the Atlantic. We compare these data with new results acquired through an improved LC method able to distinguish between the 5- and 6-methyl

290 brGDGTs (De Jonge et al., 2013) on the soils, riverbank sediments, and SPM samples
291 previously obtained by Zell et al., (2014).

292

293 **3.1 Bulk parameters of the sediments**

294 The age-depth models for the marine sediment cores (Fig. S2, Table 1) are based on
295 radiocarbon dating of picked foraminifera, gastropods, and shell fragments. The data show
296 that of the four sediment cores from the transect the Tagus River Floodplain sediments date to
297 6.7 cal. kyrs. BP, the Mudbelt sediments date to 5.8 cal. kyrs. BP, the Lisbon Canyon Head
298 sediments date to 8.7 cal. kyrs. BP, and the Lower Setúbal Canyon penetrated the oldest strata
299 (13.0 cal. kyrs. BP). Reported values for sediments from each location were averaged over the
300 interval 0-6.0 cal. kyrs. BP, so as to avoid a bias in the data since not all of the sediment cores
301 covered more than 6.0 kyrs.

302 The bulk carbon isotope data for the Tagus River SPM, riverbank sediments, and soils
303 has been previously discussed in Zell et al., (2014). The TOC values for the Tagus River
304 Floodplain sediments are relatively high and also highly variable with a range of 1.5-16 wt. %
305 and a mean of 6.5±4.3 wt. % (average ± standard deviation) and the mean $\delta^{13}C_{TOC}$ was -
306 27.0±1.0 ‰ (Fig. 2; Table 3). In the Mudbelt sediments the TOC is less variable than in the
307 Tagus River Floodplain sediments, ranging from 0.6-1.2 wt. % and with an average of
308 0.9±0.2 wt. % (Fig. 2; Table 3). The average $\delta^{13}C_{TOC}$ in the Mudbelt sediments, -24.3±0.2 ‰,
309 is higher than in the Tagus River Floodplain sediments. The average $\delta^{13}C_{TOC}$ of the Lisbon
310 Canyon Head sediments, -23.0±0.6 ‰, is higher than the Mudbelt sediments and the TOC
311 content is similar to that of the Mudbelt sediments, ranging from 0.25-1.5 wt. % with the
312 mean of 0.9±0.3 wt. % (Fig. 2; Table 3). The average $\delta^{13}C_{TOC}$ values in the Lower Setúbal
313 Canyon sediments (-23.4±1.5‰) are similar to those of the Lisbon Canyon Head sediments

with a TOC content ranging from 0.51-0.85 wt. % with a mean value of 0.65±0.14 wt. % (Fig. 2; Table 3).

3.2 Concentrations and distributions of GDGTs

Tagus Soils and Riverbank Sediments. The average concentration of crenarchaeol is higher in the riverbank sediments (~8.7±7.8 μg gOC^{-1}) than in the soils (~1.4±1.1 μg gOC^{-1}) (Fig. 3a-b; Table 3). The same trend is true for the brGDGTs with the average concentration being higher in the riverbank sediments (~33.9±24.5 μg gOC^{-1}) than the soils (~6.8±6.5 μg gOC^{-1}) (Fig. 3a-b; Table 3). The values of the BIT index were similar to those previously reported (Zell et al., 2014) for both the soils and riverbank sediments and ranged from 0.3 to 1.0 with an average of 0.7±0.2 (Fig. 3c; Table 3). The re-analysis of the brGDGTs in the soils reveals that the relative abundance of the novel 6-methyl brGDGTs is highly variable (ranging from 0.13-0.92) and can be quite high; the average values for the IR are 0.6±0.3 (Fig. 3e; Table 3). IR is even higher but less variable for the riverbank sediments with an average of 0.7±0.1 (Fig. 3e; Table 3). In general the penta- and hexamethylated brGDGTs show the same ratio of 5- and 6-methyl isomers (Fig. 4), however, in soils from an altitude of >350 m the 6-methyl brGDGTs are especially dominant (Fig. S3). Values for the new MBT'_{5me} index, which excludes the 6-methyl brGDGTs (cf. De Jonge et al., 2014a), of the soils and riverbank sediments are quite similar with an average of 0.5±0.1 in both cases (Fig. 3f; Table 3). The DC' ratio deviates between the soils and the riverbank sediments (Fig. 3d; Table 3). The DC' for the soils is highly variable but on average low (0.2±0.1); for the riverbank sediments it is higher with an average of 0.4±0.1 (Fig. 3d; Table 3).

Tagus River SPM. The SPM was obtained from the Tagus Estuary near the mouth of the Tagus River once a month over the course of a year (excluding the month of August).

Data from the Tagus River SPM showed that the summed brGDGT and crenarchaeol concentrations in the river SPM varied throughout the year and were on average 45±23 μg gOC^{-1}, and 9.8±6.8 μg OC^{-1}, (Figs. 3a-b; Table 3), respectively, resulting in only small variations in the BIT index (i.e. 0.8±0.1; Fig. 3c; Table 3). The distribution of brGDGTs (Fig. 5c) was relatively constant throughout the year as is evident from the values for MBT'_{5me} (0.5±0.0), DC' (0.3±0.0), and IR (0.6±0.0) for the river SPM (Figs. 3d-f; Table 3).

Tagus River Floodplain sediments. The average crenarchaeol concentration is fairly low in the Tagus River Floodplain sediments, 2.8±1.7 μg gOC^{-1}, conversely, the average sum of the brGDGTs in the sediments, 70±26 μg gOC^{-1}, is the largest out of the entire transect (Figs. 3a-b; Table 3). The BIT index is fairly high and constant throughout the sediment core with an average value of 0.9±0.0 (Fig. 3c; Table 3). The distribution of brGDGTs (Fig. 5d) is somewhat similar to that of the riverine SPM (Fig. 5c) and shows no major changes over the Holocene. The Tagus River Floodplain sediments has the lowest average values for MBT'_{5me}, 0.4±0.1, and IR, 0.4±0.0, of all the sediment records in the transect (Figs. 3e-f). The mean DC' throughout the sediments in this sample set is 0.4±0.1 (Fig. 3d; Table 3).

Mudbelt sediments. The average concentration of the brGDGTs in the mudbelt sediments, 25±14 μg gOC^{-1}, is lower than in the Tagus River Floodplain sediments, however, the concentration of crenarchaeol, 170±50 μg gOC^{-1}, is higher in the Mudbelt sediments (Figs. 3a-b; Table 3). This results in a lower mean value of the BIT index (i.e. 0.09±0.03; Fig. 3c; Table 3). The brGDGT distribution is relatively constant over the Holocene and is fairly similar to that of the Tagus River floodplain sediments with slightly higher fractional abundances of Ia and IIIa' (cf. Figs. 5d-e; Table 3). The average value of the MBT'_{5me} (0.5±0.0) is similar to the Tagus River SPM value (Fig. 3f). The average value of the DC' is 0.3±0.1 and the mean value of the IR is 0.5±0.0 (Figs. 3d-e; Table 3).

362 *Lisbon Canyon Head sediments.* The average sum of the brGDGTs, 31±9.3 μg g OC^{-1},
363 is about the same in the Lisbon Canyon Head sediments as in the Mudbelt sediments but the
364 amount of crenarchaeol, 390±130 μg gOC^{-1}, is larger in the Lisbon Canyon Head sediments
365 (Figs. 3a-b; Table 3). This results in lower BIT values (0.05±0.02) than in the Mudbelt
366 sediments (Fig. 3c; Table 3). The average brGDGT distribution (Fig. 5f) is fairly similar to
367 that of the Tagus Floodplain and Mudbelt sediments and is relatively constant over the
368 Holocene. The average of the MBT'_{5me} (0.5±0.0) is statistically identical to that in the
369 Mudbelt sediments (Fig. 3f; Table 3). However, the average IR, 0.6±0.0, and DC', 0.4±0.0,
370 are both a bit higher (Figs. 3d-e; Table 3).

371 *Lower Setúbal Canyon sediments.* The concentrations of the brGDGTs in these most
372 distal sediments are quite low, on average 16±5.5 μg OC^{-1} (Fig. 3a; Table 3), while the
373 amount of crenarchaeol in this sediment core is the highest out of the entire transect at
374 470±200 μg gOC^{-1} (Fig. 3b; Table 3). This results in a low average BIT index value of
375 0.02±0.01 (Fig. 3c; Table 3). The average distribution of brGDGTs in these sediments (Fig.
376 5g) is different from the marine sediments from the other two sites, with a higher fractional
377 abundance of IIIa'. However, another component with the same molecular ion eluted at
378 around the same time as IIIa' in the Lower Setúbal Canyon sediments (which we determined
379 was not the "mixed 5,6-dimethyl isomer"; cf. Weber et al., 2015), complicating integration
380 and quantification. This indicates that the brGDGT results from these sediments must be
381 interpreted with some caution. The average MBT'_{5me} (0.6±0.1) and DC' (0.4±0.1) are fairly
382 similar to the Lisbon Canyon Head sediments averages but the average IR (0.7±0.0) is the
383 highest of all sediments (Figs. 3d-f; Table 3).

384

385 **3.3 PCA**

In order to determine the variation in the distribution of brGDGTs, we performed principal component analysis (PCA) on the distributions of brGDGTs of all the samples examined. Most variation is explained by principal component 1 (PC1; 29.8 %) and is clearly related to the fractional abundance of the 5-methyl versus 6-methyl brGDGTs (Fig. 6a). With the exception of IIIc (which is typically a minor brGDGT with a fractional abundance of <1 %; Fig. 5), all of the 5-methyl brGDGTs score positively on PC1 and the 6-methyl brGDGTs score negatively. For the overall data set, PC1 is highly negatively correlated with the IR ratio (Fig. 7a, R^2=0.78). PC2 explains 25.6 % of the variance of the PCA. Branched GDGTs that score positively on PC2 are generally comprised of cyclized and more methylated brGDGTs (Fig. 6a). With the exception of IIIc (which is typically a minor brGDGT with a fractional abundance of <1 %; Fig. 4), all of the tetra- and penta-methylated brGDGTs containing no cyclopentane moiety (i.e. Ia, IIa, and IIa') score negatively on PC2. Consequently, PC2 is highly positively correlated with DC' for the whole data set (Fig. 7b, R^2=0.84).

4. Discussion

4.1 Environmental parameters affecting brGDGT distribution in Tagus soils

Evident from the earlier study by Zell et al. (2014) was that the distribution of the brGDGTs in Tagus soils varies widely. The primary environmental parameters influencing brGDGT distributions in soil (Weijers et al., 2006), i.e. MAT and pH, did differ substantially in the Tagus River basin. MAT varies from 10-17°C and pH from 5.5-8.6 (Zell et al., 2014) and both parameters show a distinct correlation with altitude (R^2=0.93 and 0.73, respectively). Applying the brGDGT global soil calibration of Peterse et al. (2012), Zell et al. (2014) arrived at unrealistically low (0-10°C) estimated MATs using the brGDGT distributions. This was attributed to the arid conditions in the region (MAP<800 mm yr^{-1}), which has in other studies,

410 including one that analyzed soils from the Iberian peninsula, been indicated as a likely cause
411 for the discrepancy between actual and reconstructed MAT using brGDGT distributions
412 (Peterse et al., 2012; Dirghangi et al., 2013; Menges et al., 2014). Our re-analysis of the soils
413 taking into account the novel 6-methyl brGDGTs now provides the possibility to re-evaluate
414 these data. It is clear that the fractional abundances of the novel 6-methyl brGDGTs vary to a
415 large extent. The IR_{II} and IR_{III} vary from 0.1 to 0.9 (Fig. 4) and some of the soils score very
416 negatively on PC1 (Fig. 6b), which is predominantly determined by the fractional abundance
417 of the 6-methyl brGDGTs. From the global soil brGDGT dataset (De Jonge et al., 2014a) it
418 was evident that the main factor influencing the fractional abundance of the 6-methyl
419 brGDGTs is soil pH with an increased abundance in high pH soils. In the Tagus River basin
420 soil pH indeed shows a large variation, i.e. from 5.5 to 8.6, and this likely explains the large
421 variation in IR. When we calculate the pH from the brGDGT distribution using the new
422 equation (9) of De Jonge et al. (2014a), which is based predominantly on the fractional
423 abundances of 6-methyl brGDGTs, we find a highly significant correlation between measured
424 and reconstructed pH (R^2=0.89) following the 1:1 line (Fig. 8a). Differences in soil pH also
425 affect the degree of cyclization of brGDGTs (Weijers et al., 2007a; De Jonge et al., 2014b)
426 and indeed we find a significant positive correlation between DC' and soil pH (R^2=0.74). The
427 effect of MAT is not clearly revealed in the dataset. For the global soil brGDGT dataset a
428 strong relationship exists between MAT and MBT'_{5Me} (De Jonge et al., 2014a). Although we
429 observe substantial variation for MBT'_{5Me} in soils (i.e. 0.3-0.7; Fig. 3f) for this dataset, we do
430 not observe a statistically significant relationship of MAT with MBT'_{5Me}. Also, reconstructed
431 MATs are far too low, i.e. 0.5–13°C using equation (6) and 2.6–11°C using equation (10).
432 Evidently, the "cold bias" of the brGDGT distributions in the soils of the Tagus river basin
433 (Zell et al., 2014) is not solved when 5- and 6-methyl brGDGTs are individually quantified.

Previously it was postulated that in this region aquatic in-situ production and arid conditions are complicating the use of brGDGTs for climate reconstructions (Menges et al., 2014; Zell et al., 2014). Within the soil sample set a strong negative relationship exists between the DC' and the measured MAT in the Tagus basin (R^2=0.79), whereas the degree of cyclization up until this point has only been reported to be related to pH and not to MAT (Weijers et al., 2007a). Conversely, though, the MAT_{mrs} reconstructed values for the soils have a positive correlation with DC' (R^2=0.51) and it is lower than with the measured MAT. Although at this point we are unsure if this association occurs in other arid areas as well, we do believe this strong relationship between the DC' and the MAT could be affecting the applicability of brGDGTs for temperature reconstructions in this region.

4.2 Provenance of brGDGTs in the Tagus River and its outflow

The application of brGDGTs in marine sediments influenced by river outflows for reconstruction of the continental paleoclimate (e.g. Weijers et al., 2006) rests on the premise that the distribution of the brGDGTs produced in the soils must be conserved throughout riverine transport to the sediments where they are archived. Therefore, we compare brGDGT distributions and concentrations from the rest of the sample set in the source-to-sink transect to determine if the soil signal is conserved during transport in the Tagus River basin. The PCA results (Fig. 6b) indicate that for the most part the distribution of brGDGTs from the river SPM and sediments along the transect is not similar to those from the soils or the Tagus Watershed. Sediments from three of the sample sets in the transect, the Tagus River Floodplain sediments, the Mudbelt sediments and the Lisbon Canyon Head sediments, all plot differently from the soils, and although the distributions of the Lower Setúbal Canyon sediments and the Tagus River SPM plot closer, there is still an offset from the soils. The

458 Tagus Riverbank sediments plot the most closely to that of the soils in the Tagus River basin,
459 however, again a slight offset still exists. So, even without considering the effects of
460 environmental parameters on brGDGT distributions, we can already conclude that the
461 brGDGTs in the sediments and river SPM only reflect the distribution of brGDGTs in the
462 Tagus soils by a minor extent and, thus, it is unlikely that Tagus soils are a major source for
463 brGDGTs in the marine sediments.

464 Using PCA (Fig. 6) we tried to determine what factors are causing the variation in the
465 distribution of brGDGTs in the Tagus River basin. PC1 is primarily related to the
466 predominance of 5-methyl versus 6-methyl brGDGTs (Fig. 6a) and thus pH (cf. De Jonge et
467 al., 2014a). This was confirmed for the soil data set where the calculated pH based on the
468 fractional abundance of predominantly 6-methyl brGDGTs shows a good correspondence
469 with measured pH (see Sect. 5.1). De Jonge et al. (2014b) showed that in the SPM of the
470 alkaline waters of the river Yenisei 6-methyl brGDGTs also predominate, indicating that pH
471 in all kinds of environmental settings determines the ratio between 5 and 6-methyl brGDGTs.
472 The Tagus riverbank sediments, river SPM and the Lower Setúbal Canyon sediments score
473 mostly negatively on PC1 as do soils from higher altitudes (>350 m) (Fig. 6b). The Mudbelt
474 sediments, Lisbon Canyon Head sediments, the Tagus River Floodplain sediments, and the
475 lower altitude soils (<350 m) have similar abundances of the 5- and 6-methyl brGDGTs or
476 higher abundances of the 5-methyl brGDGTs and plot mostly positively on PC1. Since the
477 Tagus River Floodplain sediments, the Mudbelt sediments, and the Lisbon Canyon Head
478 sediments do not have a predominance of 6-methyl brGDGTs, this indicates that either they
479 received an equal contribution of soil derived organic matter from the lower altitude soils in
480 the region (<350 m) as from the higher altitude region (>350m) or, more likely, that in-situ
481 production of brGDGTs is a large source of brGDGTs in these sample sets.

PC2 also explains a substantial part of the variance in the dataset (25.6 %, Fig. 6b) and is correlated with DC' (R^2=0.84, n=109, Fig. 7b). Since pH is also the main driver of DC' (Weijers et al., 2007a), it suggests that differences in pH are also responsible for the variance seen in PC2. The samples that standout are the sediments from the Lower Setúbal Canyon core, which are the most marine sediments in the sample set, and plot most positively, and the lowest altitude soils (28-344 m), which plot the most negatively. These latter soils are characterized by a low measured pH. The oldest (11.6-13.0 kys BP) sediments of the Lower Setúbal Canyon score most positively on PC2. A high degree of cyclization of brGDGTs has been observed previously in marine sediments from a Svalbard fjord and attributed to marine in-situ production in the alkaline pore waters of marine sediments (Peterse et al., 2009; Weijers et al, 2014). Re-analysis of the Svalbard sediments for brGDGTs actually showed that this cyclization affects the tetra- and pentamethylated brGDGTs to a much larger extent than that of the hexamethylated brGDGTs (Sinninghe Damsté, 2016) and the same observation can be made for the sediments of the Lower Setúbal Canyon (Fig. 5g). Evidently, the high degree of cyclization of brGDGTs as a response to pH is not as clearly seen in the soils since the high altitude, high pH soils from the Tagus watershed (Fig. S3c) do not exhibit the pattern (i.e. fractional abundance of IIb' larger than that of IIa') observed in the Lower Setúbal Canyon sediments (Fig. 5g). This pattern is, to a lesser degree, also seen in the sediments of the Lisbon Canyon Head core (Fig. 5f). As mentioned earlier, the Lower Setúbal Canyon sediments also display a predominance of 6-methyl brGDGTs over the 5-methyl counterparts, especially with regards to the hexamethylated brGDGTs. In the Lower Setúbal Canyon sediments IIIa' is by far the most abundant brGDGT, consisting of 29 % of the entire brGDGT pool (Fig. 5g). This is comparable to Svalbard sediments (Sinninghe Damsté, 2016) where IIIa' is also the most abundant brGDGT. Taken together this clearly indicates the influence of in-situ production in the Lower Setúbal Canyon sediments. However, the degree

of cyclization for Ia-c and IIa-c is not as high as observed for the Svalbard sediments, which still suggests some allochthonous input of brGDGTs even in these remote marine sediments.

Another way to determine if in-situ production is a factor affecting the brGDGT distribution in aquatic environments is by the calculation of reconstructed pH values. If in-situ production is heavily contributing to the brGDGT pool, then the reconstructed pH values should reflect that of the aquatic environment in which they were produced. The average reconstructed pH of the sample sets in the transect are relatively high with a clear trend to higher values with increasing distance from the river mouth (Fig. 9a), which would be in line with increased in situ production of brGDGTs in the alkaline pore waters of marine sediments. However, these values are still within the range of the measured (5.5-8.5) and reconstructed (Fig. 9a) pH of the soils and so this does not prove in-situ production as a major contributor of brGDGTs in these sample sets. Conversely, the newly calculated DC', also a reflection of pH, is quite variable throughout the sample sets in the transect except for in the river SPM where it is fairly constant (Fig. 3d; Table 3). Since the DC' is lowest in the soils (0.2±0.1) and then higher in the rest of the samples in the transect (0.3-0.4), this suggests in-situ production is an issue (cf. Zell et al., 2014) in all of the sample sets (Fig. 3d; Table 3).

4.3 brGDGTs as indicators of terrestrial OM transport by the Tagus River

Classically, the assessment of the contribution of terrestrial OM to marine sediments is performed by measuring $\delta^{13}C_{TOC}$ (Hedges and Oades, 1997 and references cited therein). In the earlier study of the Tagus River system, Zell et al. (2014) determined that the average $\delta^{13}C_{TOC}$ of the riverine SPM (~-29 ±0.8‰), like the Tagus soils, are consistent with a predominant C_3 higher plants origin (Fry and Sherr, 1984). Additionally, this study found the $\delta^{13}C_{TOC}$ in marine surface sediments off the Portuguese coast in front of the Tagus River

increase with increasing distance offshore by an increased contribution of ^{13}C-enriched marine OM. This trend is also evident for the Holocene sediments studied here. The most terrestrial sediments of the transect, i.e. from the Tagus River Floodplain, also have a $\delta^{13}C_{TOC}$ value (~27±1.0 ‰; Fig. 2a; Table 3) consistent with a predominant C_{origin} of higher plants. Moving offshore, the less negative $\delta^{13}C_{TOC}$ values of the Mudbelt sediments (-24±0.2 ‰), the Lisbon Canyon Head sediments (-23±0.6 ‰) and the Lower Setúbal Canyon sediments (-23±1.5 ‰) all indicate that the majority of the TOC off the Portuguese shelf is of marine origin (Fig. 2a; Table 3). So, as Zell et al. (2014) found with marine surface sediments off the Portuguese coast, the $\delta^{13}C_{TOC}$ (‰) averages from the sediments in our transect also increase with increasing distance offshore, demonstrating that the present trend in the $\delta^{13}C_{TOC}$ signal remained the same over the Holocene.

Zell et al. (2014) previously showed that in the present day Tagus River system the amount of brGDGTs (µg gOC^{-1}) increases from the soils to the riverbank sediment to the river SPM and explained this increase as proof of riverine in-situ production of brGDGTs. Concentrations of summed brGDGTs in surface sediments in transects from the Portuguese coast rapidly declined with increasing distance from the coast, suggesting that brGDGTs could still be used as tracer for terrestrial organic matter (Zell et al., 2015). The trends observed in these earlier studies are confirmed here for the Holocene. The Tagus River Floodplain sediments have the highest concentration of brGDGTs (67±26 µg gOC^{-1}) in the entire transect, much higher than in the soils (Fig. 3b; Table 3). However, the sediments in this core are somewhat a-typical for the Tagus Floodplain as some layers consist of peat as a result of the low-energy backswamp conditions in the vicinity, which could explain the difference in brGDGT concentrations from the surrounding soils. This could also be due to the addition of aquatically produced brGDGTs from the river during times of flooding although it should be noted that the concentration of brGDGTs is even higher than in riverine

556 SPM (Fig. 3b). The summed brGDGT concentration decreases and is fairly similar among the
557 Mudbelt sediments (25±14 μg gOC^{-1}) and the Lisbon Canyon Head sediments (31±9.3 μg
558 gOC^{-1}), and then decreases further moving away from the coastline to the Lower Setúbal
559 Canyon sediments (16±5.5 μg gOC^{-1}) demonstrating the decrease in input of riverine
560 brGDGTs moving away from the shoreline (Fig. 3b). However, even though the sum of the
561 brGDGTs are lower in the marine sediment than in the Tagus River Floodplain sediments, the
562 amount of brGDGTs in all four sediment cores are higher than in the Tagus soils (~6.8±6.5 μg
563 gOC^{-1}) indicating the origin of the brGDGTs in the sediment cores are not all soil derived and
564 pointing instead to riverine in-situ production as well as possibly in aquatic sediments (Fig.
565 3b).

566 A previous study by Zell et al., (2015) determined that in the surface sediments off the
567 coast of Portugal the BIT index is influenced by both declining brGDGT concentrations and
568 increased crenarchaeol production with increasing distance from the coast. For the Holocene
569 sediments studied here, the average concentration of crenarchaeol in the Tagus River
570 Floodplain sediments is low (2.8±1.7 μg gOC^{-1}) and similar to that of the Tagus soils (1.4±1.1
571 μg gOC^{-1}; Fig. 3a; Table 3). The crenarchaeol concentration increases in the sediments with
572 increasing distance from the shoreline, signifying the increase in marine production with
573 water depth and distance from the coast (Fig. 3a). Consequently, the BIT index is the highest
574 in the Tagus River Floodplain sediments (0.94±0.03) out of the entire transect (Fig. 3c) and
575 then the BIT index decreases within the sediments along the transect with increasing distance
576 from the Portuguese coast potentially signifying a decrease in terrestrial input moving away
577 from the shoreline.

578 **4.4 Factors affecting the application of brGDGTs for paleoclimate reconstructions off**
579 **the Iberian Peninsula**

580 Despite the caveats with respect to in-situ production of brGDGTs in aquatic
581 environments as described in the previous section, we tested how the new soil calibration
582 based on individually quantified 5-methyl and 6-methyl brGDGTs (De Jonge et al., 2014a)
583 performed to reconstruct continental MAT in this region. For this comparison we will
584 consider the present day MAT of the entire Tagus River basin, 14.6±2.2°C (Zell et al., 2014),
585 assuming that soil derived brGDGTs from along the whole river basin are contributing to the
586 marine sediments. The assumption that the brGDGTs from the entire Tagus River basin are
587 being contributed to oceanic sediments is probably invalid for modern times as the
588 construction of dams along the Tagus River, which began in the 1940s, most likely prevents
589 part of the terrestrial material from upstream making it downstream and out off the coast of
590 Portugal. However, since we are not looking at marine surface sediments in this study but
591 instead sediments deposited during the Holocene, the placement of dams in the river should
592 not affect our results except for with the riverine SPM. Despite the separation of the 5- and 6-
593 methyl brGDGT isomers and the application of the new proxy, the reconstructed MATs using
594 both riverine SPM and Holocene sediments is still substantially lower than 14.6°C (Figs. 9b
595 and 9c), as noted for the soils (see Sect. 5.1). Using the MAT_{mr} calibration the Lisbon Canyon
596 Head sediments the average temperature (12.4±0.5°C) comes closest to the modern day MAT
597 in the region and using the MAT_{mrs} calibration the Lower Setúbal Canyon sediments
598 (11.2±0.7°C) has the most similar average temperature (Figs. 9b and 9c).

599 Even though we used the new calibration to reconstruct MAT, it should be noted that
600 the low BIT values (<0.15; Fig. 3c) of the Holocene sediments deposited at the three marine
601 sites indicates that there were probably not enough soil-derived brGDGTs making it out to
602 ocean and being deposited in the sediments over the Holocene for reliable climate
603 reconstructions (cf. Weijers et al., 2014). By looking at the summed concentration of
604 brGDGTs along the entire transect, it is apparent that since it is lowest in the soils that

605 although the BIT index seems high enough for MAT reconstructions in the riverbank
606 sediments and river SPM, the origin of the brGDGTs may not be solely soil derived and this
607 could be complicating reconstructions throughout the transect as was discussed previously
608 (see Sect. 5.2). This further supports earlier conclusions from preceding studies (Yang et al.,
609 2012; Zell et al., 2013) stating that the amount and origin of brGDGTs in a system needs to be
610 examined along with the BIT index when determining if brGDGTs can be applied for MAT
611 reconstruction.

612

613 **5. Conclusions**

614 We have established that the distribution of brGDGTs varies greatly within the Tagus
615 River basin (Fig. 5) and although this may be partly explained by the varying contributions of
616 higher altitude, which contain a greater proportion of 6-methyl isomers, versus lower altitude
617 soils in the sample sets it is more likely due to the contribution of aquatically produced
618 brGDGTs in some of the sample sets. In order to use sedimentary brGDGTs for paleoclimate
619 reconstructions, the distribution of brGDGTs in the soils must be related to the MAT and
620 conserved throughout riverine transport to the sediments where they are deposited, however,
621 our results corroborate previous studies stating that most of the terrestrial matter is not making
622 it out to the ocean and being deposited in sediments close to shore. The lack of soil derived
623 OM in offshore sediments along with the substantial input of aquatically produced brGDGTs
624 is complicating MAT reconstructions from sedimentary, marine brGDGTs in this region.

625 Additionally, we confirm the findings of Zell et al., (2014; 2015) that in-situ production
626 of brGDGTs is occurring in the river and marine systems of the Tagus River basin and go on
627 to show that there are indications that it occurred in the past as well. Although in-situ
628 production is complicating environmental reconstructions using marine sediments, another

629 issue is that accurate MAT reconstructions using brGDGTs cannot currently be performed on
630 the soils, even with the separation of the 6-methyl brGDGTs from the 5-methyl isomers using
631 the new method and calibrations. Previous studies have concluded that paleoclimate
632 reconstructions in arid regions using brGDGTs are complicated due to a breakdown in the
633 relationship with MBT' and MAT (Peterse et al., 2012; Menges et al., 2014). In this study we
634 confirm that there is not a strong relationship between the MBT'_{5me} and measured MAT in
635 this arid region. However, we also do not observe the same relationship with MAP and
636 MBT'_{5me} that has been previously reported between MAP and MBT' in arid regions and has
637 been implicated in making reconstructions difficult. Instead, we see a strong relationship with
638 the DC' and measured MAT in the area not observed before. We also see a predominance of
639 6-methyl isomers, previously only reported in river SPM, in the Tagus soils from greater than
640 350 m altitude. Although this might be a characteristic of arid soils and related to MAP since
641 it is below 550 mm yr^{-1} in most of the soil samples above 350 m, the two highest elevation
642 soil samples, which both have a MAP above 550 mm yr^{-1}, also demonstrate this trend. Future
643 studies need to be performed in arid environments to determine if a strong relationship
644 between MAT and DC' as well as a predominance of 6-methyl isomers are characteristics of
645 arid regions and contributing to the complications found using brGDGTs for paleoclimate
646 reconstructions. Also, higher elevation environments should be further studied to determine if
647 a predominance of 6-methyl brGDGTs is a feature of higher altitudes and complicating
648 climate reconstructions.

649 Because of these unique features in this region, perhaps the development of a local
650 calibration could assuage difficulties in using brGDGTs as a paleoclimate proxy for soils in
651 the Tagus River basin. This would not, however, solve the issue of in-situ produced brGDGTs
652 overwhelming the amount of soil derived brGDGTs in aquatic sediments. We did find that the
653 new CBT' and pH calibration do an excellent job reconstructing pH in the soils of the Tagus

basin and since pH is related to other environmental factors such as MAP this will be useful for paleoclimate reconstructions in terrestrial sites over the Iberian peninsula where in-situ production is not a complicating factor.

Author contribution

J.H. Kim and J.S.S. Damsté designed the study, which was carried out by L. Warden who completed bulk carbon isotope and brGDGT analysis on samples along with C. Zell. C. Zell, H. Stigter, G.J. Vis and J.H. Kim collected samples for this study. J. Bonnin picked forams for dating. L. Warden and J.S.S. Damsté prepared the manuscript with contributions from all co-authors.

Acknowledgements

The research leading to these results has received funding from the European Research Council under the European Union's Seventh Framework Programme (FP7/2007-2013) / ERC grant agreement n° [226600]. JSSD is supported by funding from the Netherlands Earth System Science Center (NESSC) though a gravitation grant from the Dutch ministry for Education, Culture and Science. We thank the captain and crew of the R/V Pelagia for their support with sampling. We thank J. Ossebaar and E.C. Hopmans for their help with the HPLC-APCI-MS analysis, J. Ossebaar for his help with the element analyzer, and L.A.C. Rosales and A. Mets for help with sample preparation.

Data Availability

The data presented in this paper can be found in Table 3 and S2.

677 **Figure captions**

678 **Figure 1** The location of the study area on the Iberian Peninsula with the stations where the
679 four sediment cores were sampled (indicated by black squares) along a transect from the
680 Tagus River to off the Portuguese continental margin as well as the river SPM sampling site
681 (indicated by a white diamond), riverbank sediment sampling sites (indicated by red circles),
682 and soil sampling sites (indicated by black circles). The River SPM, riverbank sediments and
683 soil samples were all collected for a previous study. Digital elevation data from Jarvis et al.
684 (2006) and bathymetry from IOC-IHO-BODC (2003).

685 **Figure 2** Boxplots of (a) $\delta^{13}C_{TOC}$ (‰) of the organic carbon and (b) TOC (wt. %) for each
686 sample set along the Tagus River source to sink transect. The increasing $\delta^{13}C_{TOC}$ values in the
687 sediment core locations with increasing distance from the coast indicates that more of the
688 organic carbon in these sediments is marine derived.

689 **Figure 3** Boxplots of (a) crenarchaeol concentrations (µg gOC^{-1}), (b) sum of brGDGTs (µg
690 gOC^{-1}), (c) BIT index, (d) DC', (e) IR, (f) MBT'_{5me} for each sample set in the transect from
691 the land to the ocean off the Portuguese coast.

692 **Figure 4** Isomer ratio for the non-cyclized pentamethylated brGDGT (IR_{II}) plotted against
693 that of the non-cyclized hexamethylated brGDGT (IR_{III}).

694 **Figure 5** Average distribution of brGDGTs for each sample set along the transect of samples
695 that runs from the land to the ocean off the coast of Lisbon. Evident from this figure is that the
696 distribution of brGDGTs within this sample set varies greatly. Distributions of brGDGTs in
697 marine sediments only reflects the distribution of the brGDGTs from the Tagus soils to a
698 minor extent. The color of the bars reflects the brGDGT structure as labeled in the legend and
699 the range indicated with the error bars equals 2xs the standard deviation.

Figure 6 Principal component analysis based on the fractional abundances of the 15 brGDGTs of samples in the transect that runs from inland to off the coast of Portugal plotting a) the scores of the brGDGT compounds on the first two principal components (PC) and b) the scores of the samples from each sample set used in this study.

Figure 7 Scatter plots of (a) PC1 against the IR (R^2=0.78) and (b) PC2 against DC' (R^2=0.84) for the entire set of samples used in this study.

Figure 8 Panels a-c show scatterplots of the Tagus soil samples for a) reconstructed and measure pH (R^2=0.89), b) reconstructed MAT_{mr} (°C) and measured MAT (°C) (R^2=0.27), c) reconstructed MAT_{mrs} (°C) and measured MAT (°C) (R^2=0.38). For panels b-c the soil samples from an altitude greater than 350m are indicated in black and those from an altitude below 350m are indicated in green. Panels d-f show scatter plots of the Tagus riverbank sediments for d) reconstructed and measured pH (R^2=0.14), e) reconstructed MAT_{mr} (°C) and measured MAT (°C) (R^2=0.31), f) reconstructed MAT_{mrs} (°C) and measured MAT (°C) (R^2=0.23). Panel g is a scatter plot showing the reconstructed and measured pH for the Tagus River SPM samples (R^2=0.09).

Figure 9 Boxplots of all the sample sets within the transect from the land to the deep ocean off the Portuguese coast for (a) reconstructed pH, (b) MAT_{mrs} (°C) and (c) MAT_{mr} (°C). Red dotted line indicates estimated present day MAT for the Tagus River basin (14.6°C).

References

Abrantes, F., Lebreiro, S., Rodrigues, T., Gil, I., Bartels-Jónsdóttir, H., Oliveira, P., Kissel, C., and Grimalt, J.O.: Shallow-marine sediment cores record climate variability and earthquake activity off Lisbon (Portugal) for the last 2000 years, Quat. Sci. Rev., 24, 2477–2494, 2005.

724 Abrantes, F., Lopes, C., Rodrigues, T., Gil, I., Witt, L., Grimalt, J., and Harris, I.: Proxy
725 calibration to instrumental data set: Implications for paleoceanographic reconstructions,
726 Geochem. Geophys. Geosyst., 10, Q09U07, doi:10.1029/2009GC002604, 2009.

727 Andreu, L., GutiéRrez, E., Macias, M., Ribas, M., Bosch, O., and Camarero, J.J.: Climate
728 increases regional tree-growth variability in Iberian pine forests, Glob. Change Biol., 13, 1-
729 12, 2007.

730 Bartels-Jónsdóttir, H.B., Knudsen, K.L., Abrantes, F., Lebreiro, S., and Eiríksson, J.: Climate
731 variability during the last 2000 years in the Tagus Prodelta, western Iberian Margin: Benthic
732 foraminifera and stable isotopes, Mar. Micropaleontol., 59, 83–103, 2006.

733 Bartels-Jonsdottir, H.B., Voelker, A.H.L., Knudsen, K.L., and Abrantes, F.: Twentieth-
734 century warming and hydrographical changes in the Tagus Prodelta, eastern North Atlantic,
735 Holocene, 19, 369–380, 2009.

736 Bendle, J.A., Weijers, J.W., Maslin, M.A., Sinninghe Damsté, J.S., Schouten, S., Hopmans,
737 E.C., Boot, C.S., and Pancost, R.D.: Major changes in glacial and Holocene terrestrial
738 temperatures and sources of organic carbon recorded in the Amazon fan by tetraether lipids,
739 Geochem. Geophys. Geosyst., 11, Q12007, doi:10.1029/2010GC003308, 2010.

740 Benito, G., Díez-Herrero, A., and de Villalta, M.F.: Magnitude and frequency of flooding in
741 the Tagus basin (Central Spain) over the last millennium, Clim. Change, 58, 171–192, 2003.

742 Cachao, M., and Moita, M.T.: *Coccolithus pelagicus,* a productivity proxy related to moderate
743 fronts off Western Iberia, Mar. Micropaleontol., 39, 131–155, 2000.

744 Corella, J.P., Stefanova, V., El Anjoumi, A., Rico, E., Giralt, S., Moreno, A., Plata-Montero,
745 A., and Valero-Garcés, B.L.: A 2500-year multi-proxy reconstruction of climate change and
746 human activities in northern Spain: The Lake Arreo record, Palaeogeogr. Palaeoclimatol.
747 Palaeoecol. , 386, 555–568, 2013.

748 Davis, B.A.S., Brewer, S., Stevenson, A.C., and Guiot, J.: The temperature of Europe during
749 the Holocene reconstructed from pollen data, Quatern. Sci. Rev., 22, 1701–1716, 2003.

750 De Jonge, C., Hopmans, E.C., Stadnitskaia, A., Rijpstra, W.I.C., Hofland, R., Tegelaar, E.,
751 and Sinninghe Damsté, J.S.: Identification of novel penta-and hexamethylated branched
752 glycerol dialkyl glycerol tetraethers in peat using HPLC–MS^2, GC–MS and GC–SMB-MS.
753 Org. Geochem., 54, 78–82, 2013.

754 De Jonge, C., Hopmans, E.C., Zell, C.I., Kim, J.-H., Schouten, S., and Sinninghe Damsté,
755 J.S.: Occurrence and abundance of 6-methyl branched glycerol dialkyl glycerol tetraethers in
756 soils: Implications for palaeoclimate reconstruction. Geochim. Cosmochim. Acta, 141, 97–
757 112, 2014a.

758 De Jonge, C., Stadnitskaia, A., Hopmans, E.C., Cherkashov, G., Fedotov, A., and Sinninghe
759 Damsté, J.S.: In situ produced branched glycerol dialkyl glycerol tetraethers in suspended
760 particulate matter from the Yenisei River, Eastern Siberia, Geochim. Cosmochim. Acta, 125,
761 476–491, 2014b.

762 De Jonge, C., Stadnitskaia, A., Hopmans, E.C., Cherkashov, G., Fedotov, A., Streletskaya,
763 I.D., Vasiliev, A.A., and Sinninghe Damsté, J.S.: Drastic changes in the distribution of

764 branched tetraether lipids in suspended matter and sediments from the Yenisei River and Kara
765 Sea (Siberia): Implications for the use of brGDGT-based proxies in coastal marine sediments,
766 Geochim. Cosmochim. Acta, 165, 200-225, 2015.

767 Dias, J.M.A., Jouanneau, J.M., Gonzalez, R., Araújo, M.F., Drago, T., Garcia, C., Oliveira,
768 A., Rodrigues, A., Vitorino, J., and Weber, O.: Present day sedimentary processes on the
769 northern Iberian shelf, Prog. Oceanogr., 52, 249–259, 2002.

770 Dirghangi, S.S., Pagani, M., Hren, M.T., and Tipple, B.J.: Distribution of glycerol dialkyl
771 glycerol tetraethers in soils from two environmental transects in the USA, Org. Geochem., 59,
772 49–60, 2013.

773 Fletcher, W.J., Boski, T., and Moura, D.: Palynological evidence for environmental and
774 climatic change in the lower Guadiana valley, Portugal, during the last 13,000 years,
775 Holocene, 17, 481–494, 2007.

776 Fry, B., and Sherr, E.: $\delta^{13}C$ measurements as indicators of carbon flow in marine and
777 freshwater ecosystems, Contrib. Mar. Sci., 27, 15–47, 1984.

778 Haug, G.H., Günther, D., Peterson, L.C., Sigman, D.M., Hughen, K.A., and Aeschlimann, B.:
779 Climate and the collapse of Maya civilization, Science, 299, 1731–1735, 2003.

780 Hedges, J.I., and Oades, J.M.: Comparative organic geochemistries of soils and marine
781 sediments, Org. Geochem., 27, 319–361, 1997.

782 Hopmans, E.C., Schouten, S., and Sinninghe Damsté, J.S.: The effect of improved
783 chromatography on GDGT-based palaeoproxies, Org. Geochem., 93, 1-6, 2015.

784 Hren, M.T., Pagani, M., Erwin, D.M., and Brandon, M: Biomarker reconstruction of the early
785 Eocene paleotopography and paleoclimate of the northern Sierra Nevada, Geology, 38, 7–10,
786 2010.

787 Huguet, C., Hopmans, E.C., Febo-Ayala, W., Thompson, D.H., Sinninghe Damsté, J.S., and
788 Schouten, S.: An improved method to determine the absolute abundance of glycerol
789 dibiphytanyl glycerol tetraether lipids, Org. Geochem., 37, 1036–1041, 2006.

790 Huntley, B., and Prentice, I.C.: July temperatures in Europe from pollen data, 6000 years
791 before present, Science, 241, 687–690, 1988.

792 Hurrell, J.W.: Decadal trends in the North Atlantic oscillation, Science, 269, 676–679, 1995.

793 Hurrell, J.W., and Van Loon, H: Decadal variations in climate associated with the north
794 Atlantic oscillation, Clim. Change, 36, 301–326, 1997.

795 International Ocean Commission, International Hydrographic Organization, and British
796 Oceanographic Data Centre (IOC/IHO/BODC): Centenary Edition of the GEBCO Digital
797 Atlas, Published on CD-ROM on Behalf of the Intergovernmental Oceanographic
798 Commission and the International Hydrographic Organization as part of the General
799 Bathymetric Chart of the Oceans, British-Oceanographic-Data-Centre (Ed.), Liverpool,
800 United Kingdom, 2003.

801 Jarvis, A., Reuter, H.I., Nelson, A., Guevara, E.: Hole-filled seamless SRTM data vol. 3,
802 International Centre for Tropical Agriculture (CIAT), 2006.

803 Jesus, C.C., de Stigter, H.C., Richter, T.O., Boer, W., Mil-Homens, M., Oliveira, A., and
804 Rocha, F.: Trace metal enrichments in Portuguese submarine canyons and open slope:
805 anthropogenic impact and links to sedimentary dynamics, Mar. Geol., 271, 72–83, 2010.

806 Jouanneau, J.M., Garcia, C., Oliveira, A., Rodrigues, A., Dias, J.A., and Weber, O.: Dispersal
807 and deposition of suspended sediment on the shelf off the Tagus and Sado estuaries, SW
808 Portugal. Prog. Oceanogr. 42, 233–257, 1998.

809 Keating-Bitonti, C.R., Ivany, L.C., Affek, H.P., Douglas, P., and Samson, S.D.: Warm, not
810 super-hot, temperatures in the early Eocene subtropics, Geology, 39, 771–774, 2011.

811 Lastras, G., Arzola, R.G., Masson, D.G., Wynn, R.B., Huvenne, V.A.I., Hühnerbach, V., and
812 Canals, M.: Geomorphology and sedimentary features in the Central Portuguese submarine
813 canyons, Western Iberian margin, Geomorphology, 103, 310–329, 2009.

814 Lebreiro, S.M., Francés, G., Abrantes, F.F.G., Diz, P., Bartels-Jónsdóttir, H.B., Stroynowski,
815 Z.N., Gil, I.M., Pena, L.D., Rodrigues, T., and Jones, P.D.: Climate change and coastal
816 hydrographic response along the Atlantic Iberian margin (Tagus Prodelta and Muros Ría)
817 during the last two millennia, Holocene, 16, 1003–1015, 2006.

818 Le Pera, E., and Arribas, J.: Sand composition in an Iberian passive-margin fluvial course: the
819 Tajo River, Sediment. Geol., 171, 261–281, 2004.

820 Linan, I.D., Gutierrez, E., Andreu-Hayles, L., Heinrich, I., and Helle, G.: Potential to explain
821 climate from tree rings in the south of the Iberian Peninsula, Clim. Res., 55, 119–134, 2012.

822 Martin-Chivelet, J., Belen Munoz-Garcia, M., Edwards, R.L., Turrero, M.J., and Ortega, A.I.:
823 Land surface temperature changes in Northern Iberia since 4000 yr BP, based on delta C-13
824 of speleothems, Glob. Planet. Change, 77, 1–12, 2011.

825 Menges, J., Huguet, C., Alcañiz, J.M., Fietz, S., Sachse, D., and Rosell-Melé, A.: Influence of
826 water availability in the distributions of branched glycerol dialkyl glycerol tetraether in soils
827 of the Iberian Peninsula, Biogeosciences, 11, 2571-2581, 2014.

828 Munoz-Garcia, M.B., Martin-Chivelet, J., Rossi, C., Ford, D.C., and Schwarcz, H.P.:
829 Chronology of termination II and the Last Interglacial Period in North Spain based on stable
830 isotope records of stalagmites from Cueva del Cobre (Palencia), J. Iber. Geol., 33, 17–30,
831 2007.

832 Palumbo, E., Flores, J.A., Perugia, C., Emanuele, D., Petrillo, Z., Rodrigues, T., Voelker,
833 A.H., and Amore, F.O.: Abrupt variability of the last 24 ka BP recorded by coccolithophore
834 assemblages off the Iberian Margin (core MD03-2699), J. Quatern. Sci., 28, 320–328, 2013.

835 Pancost, R.D., and Sinninghe Damsté, J.S.: Carbon isotopic compositions of prokaryotic
836 lipids as tracers of carbon cycling in diverse settings, Chem. Geol., 195, 29–58, 2003.

837 Peterse, F., Kim, J.-H., Schouten, S., Kristensen, D.K., Kocc, N., and Sinninghe Damsté, J.S.:
838 Constraints on the application of the MBT/CBT palaeothermometer at high latitude
839 environments (Svalbard, Norway), Org. Geochem., 40, 692–699, 2009.

Peterse, F., Meer, J. van der, Schouten, S., Weijers, J.W., Fierer, N., Jackson, R.B., Kim, J.-H., and Sinninghe Damsté, J.S.: Revised calibration of the MBT-CBT paleotemperature proxy based on branched tetraether membrane lipids in surface soils, Geochim. Cosmochim. Acta, 96, 215-229, 2012.

Reimer, P.J., Bard, E., Bayliss, A., Beck, J.W., Blackwell, P.G., Ramsey, C.B., Buck, C.E., Cheng, H., Edwards, R.L., Friedrich, M. and Grootes, P.M. : IntCal13 and Marine13 radiocarbon age calibration curves 0-50,000 years cal BP, Radiocarbon, 55, 1869-1887, 2013.

Rodó, X., Baert, E., and Comín, F.A.: Variations in seasonal rainfall in Southern Europe during the present century: relationships with the North Atlantic Oscillation and the El Niño-Southern Oscillation, Clim. Dynam., 13, 275–284, 1997.

Rodrigues, T., Grimalt, J.O., Abrantes, F.G., Flores, J.A., and Lebreiro, S.M.: Holocene interdependences of changes in sea surface temperature, productivity, and fluvial inputs in the Iberian continental shelf (Tagus mud patch), Geochem. Geophys. Geosyst., 10, Q07U06, doi:10.1029/2008GC002367, 2009.

Schouten, S., Eldrett, J., Greenwood, D.R., Harding, I., Baas, M., and Sinninghe Damsté, J.S.: Onset of long-term cooling of Greenland near the Eocene-Oligocene boundary as revealed by branched tetraether lipids, Geology, 36, 147–150, 2008.

Sinninghe Damsté, J.S., Schouten, S., Hopmans, E.C., van Duin, A.C., and Geenevasen, J.A.: Crenarchaeol the characteristic core glycerol dibiphytanyl glycerol tetraether membrane lipid of cosmopolitan pelagic crenarchaeota, J. Lipid Res., 43, 1641–1651, 2002.

Sinninghe Damsté, J.S., Ossebaar, J., Abbas, B., Schouten, S., and Verschuren, D.: Fluxes and distribution of tetraether lipids in an equatorial African lake: Constraints on the application of the TEX_{86} palaeothermometer and BIT index in lacustrine settings, Geochim. Cosmochim. Acta, 73, 4232–4249, 2009.

Sinninghe Damsté, J.S., Rijpstra, W.I.C., Hopmans, E.C., Weijers, J.W.H., Foesel, B.U., Overmann, J., and Dedysh, S.N.: 13,16-Dimethyl Octacosanedioic Acid (iso-Diabolic Acid), a Common Membrane-Spanning Lipid of Acidobacteria Subdivisions 1 and 3, Appl. Environ. Microbiol., 77, 4147–4154, 2011.

Sinninghe Damsté, J.S., Rijpstra, W.I.C., Hopmans, E.C., Foesel, B.U., Wüst, P.K., Overmann, J., Tank, M., Bryant, D.A., Dunfield, P.F., Houghton, K. and Stott, M.B.: Ether- and Ester-Bound iso-Diabolic Acid and Other Lipids in Members of Acidobacteria Subdivision 4, Appl. Environ. Microbiol., 80, 5207–5218, 2014.

Sinninghe Damsté, J.S.: Spatial heterogeneity of sources of branched tetraethers in shelf systems: The geochemistry of tetraethers in the Berau River delta (Kalimantan, Indonesia), Geochim. Cosmochim. Acta, 186, 13-31, 2016.

de Stigter, H.C., Jesus, C.C., Boer, W., Richter, T.O., Costa, A., and van Weering, T.C.: Recent sediment transport and deposition in the Lisbon–Setúbal and Cascais submarine canyons, Portuguese continental margin, Deep-Sea Res. Pt. II, 58, 2321–2344, 2011.

Stoll, H.M., Moreno, A., Mendez-Vicente, A., Gonzalez-Lemos, S., Jimenez-Sanchez, M., Jose Dominguez-Cuesta, M., Edwards, R.L., Cheng, H., and Wang, X.: Paleoclimate and

growth rates of speleothems in the northwestern Iberian Peninsula over the last two glacial cycles, Quatern. Res., 80, 284–290, 2013.

Stuiver, M., Reimer, P., and Braziunas, T.: High-precision radiocarbon age calibration for terrestrial and marine samples, Radiocarbon, 40, 1127–1151, 1998.

Trigo, R.M., Pozo-Vazquez, D., Osborn, T.J., Castro-Diez, Y., Gamiz-Fortis, S., and Esteban-Parra, M.J.: North Atlantic oscillation influence on precipitation, river flow and water resources in the Iberian peninsula, Int. J. Climatol., 24, 925–944, 2004.

Vale, C., and Catarino, F.: Accumulation of Zn, Pb, Cu, Cr and Ni in sediments between roots of the Tagus estuary salt marshes, Portugal, Estuar. Coast. Shelf Res., 42, 393–403, 1996.

Vaz, N., Mateus, M., and Dias, J.M.: Semidiurnal and spring-neap variations in the Tagus Estuary: Application of a process-oriented hydro-biogeochemical model, J. Coastal. Res., 64, 1619–1623, 2011.

Vis, G.-J., Kasse, C., and Vandenberghe, J.: Late Pleistocene and Holocene palaeogeography of the Lower Tagus Valley (Portugal): effects of relative sea level, valley morphology and sediment supply, Quat. Sci. Rev., 27, 1682–1709, 2008.

Vis, G.-J., and Kasse, C.: Late Quaternary valley-fill succession of the Lower Tagus Valley, Portugal, Sediment. Geol., 221, 19–39, 2009.

Vis, G.-J., Bohncke, S. J. P., Schneider, H., Kasse, C., Coenraads-Nederveen, S., Zuurbier, K. and Rozema, J.: Holocene flooding history of the Lower Tagus Valley (Portugal), J. Quat. Sci., 25, 1222-1238, 2010.

Vis, G.-J., Kasse, C., Kroon, D., Vandenberghe, J., Jung, S., Lebreiro, S.M., and Rodrigues, T.: Time-integrated 3D approach of late Quaternary sediment-depocenter migration in the Tagus depositional system: From river valley to abyssal plain, Earth-Sci. Rev., 153, 192–211, 2016.

Weber, Y., De Jonge, C., Rijpstra, W.I.C., Hopmans, E.C., Stadnitskaia, A., Schubert, C.J., Lehmann, M.F., Sinninghe Damsté, J.S., and Niemann, H.: Identification and carbon isotope composition of a novel branched GDGT isomer in lake sediments: Evidence for lacustrine branched GDGT production, Geochim. Cosmochim. Acta, 154, 118-129, 2015.

Weijers, J.W., Schouten, S., Hopmans, E.C., Geenevasen, J.A., David, O.R., Coleman, J.M., Pancost, R.D., and Sinninghe Damsté, J.S.: Membrane lipids of mesophilic anaerobic bacteria thriving in peats have typical archaeal traits. Environ. Microbiol., 8, 648–657, 2006.

Weijers, J.W., Schouten, S., van den Donker, J.C., Hopmans, E.C., and Sinninghe Damsté, J.S.: Environmental controls on bacterial tetraether membrane lipid distribution in soils, Geochim. Cosmochim. Acta, 71, 703–713, 2007a.

Weijers, J.W., Schefuß, E., Schouten, S., and Sinninghe Damsté, J.S.: Coupled thermal and hydrological evolution of tropical Africa over the last deglaciation, Science, 315, 1701–1704, 2007b.

Weijers, J.W.H., Wiesenberg, G.L.B., Bol, R., Hopmans, E.C., and Pancost, R.D.: Carbon isotopic composition of branched tetraether membrane lipids in soils suggest a rapid turnover

and a heterotrophic life style of their source organism(s), Biogeosciences, 7, 2959–2973, 2010.

Weijers, J.W.H., Bernhardt, B., Peterse, F., Werne, J.P., Dungait, J.A.J., Schouten, S., and Sinninghe Damsté, J.S.: Absence of seasonal patterns in MBT-CBT indices in mid-latitude soils, Geochim. Cosmochim. Acta, 75, 3179–3190, 2011.

Xie, S., Pancost, R.D., Chen, L., Evershed, R.P., Yang, H., Zhang, K., Huang, J., and Xu, Y.: Microbial lipid records of highly alkaline deposits and enhanced aridity associated with significant uplift of the Tibetan Plateau in the Late Miocene, Geology, 40, 291–294, 2012.

Yang, G., Zhang, C.L., Xie, S., Chen, Z., Gao, M., Ge, Z., and Yang, Z.: Microbial glycerol dialkyl glycerol tetraethers from river water and soil near the Three Gorges Dam on the Yangtze River, Org. Geochem., 56, 40-50, 2013.

Zell, C., Kim, J.-H., Moreira-Turcq, P., Abril, G., Hopmans, E.C., Bonnet, M.-P., Sobrinho, R.L., and Sinninghe Damsté, J.S.: Disentangling the origins of branched tetraether lipids and crenarchaeol in the lower Amazon River: Implications for GDGT-based proxies, Limnol. Oceanogr., 58, 343–353, 2013.

Zell, C., Kim, J.-H., Balsinha, M., Dorhout, D., Fernandes, C., Baas, M., and Sinninghe Damsté, J.S.: Transport of branched tetraether lipids from the Tagus River basin to the coastal ocean of the Portuguese margin: consequences for the interpretation of the MBT'/CBT paleothermometer, Biogeosciences, 11, 5637–5655, 2014.

Zell, C., Kim, J.-H., Dorhout, D., Baas, M., and Sinninghe Damsté, J.S.: Sources and distributions of branched tetraether lipids and crenarchaeol along the Portuguese continental margin: Implications for the BIT index, Cont. Shelf Res., 96, 34–44, 2015.

Zorita, E., Kharin, V., and Vonstorch, H.: The Atmospheric Circulation and Sea-Surface Temperature in the North-Atlantic Area in Winter - Their Interaction and Relevance for Iberian Precipitation, J. Climatol., 5, 1097–1108, 1992.

944 **Table 1** Stations, sediment core names, locations of sampling and water depth for each

945 sediment core used in this study.

Station	Core name	Latitude [N]	Longitude [W]	Water depth [m]
0501.029	Tagus River Floodplain	39° 23' 07.80"	08° 31' 55.56"	0
64PE332-30-2	Tagus Mudbelt	38° 39' 02.20”	09° 28' 07.68"	82
64PE332-44-2	Lisbon Canyon Head	38° 30' 20.19"	09° 15' 04.87"	259
64PE269-39-4	Lower Setúbal Canyon	38° 13' 12.00"	10° 10' 00.00"	4217

946

947

948

949

950

951

952

953

954

955

956

957

958

959

960 **Table 2** Summary of the data used to determine an age depth model for the sediment samples

961 in this study. [a]Data is from Vis et al., (2010).

Sediment core	Lab code	Depth in core [cm]	Mean depth in core [cm]	Uncorrected AMS^{14}C ages [yr BP]	Analytical error (±1σ) [yrs]	Ages (ΔR = 0 yr) (±2σ) [cal yr BP]	Ages [cal yr BP]	Analyzed material
0501.029[a]		0-2	1				0	
0501.029[a]		331-334	332.5	1136	38	964-1150	1057	Roots of fraction>125µm
0501.029[a]		331-334	332.5	1022	37	901-1001	951	Total organic fraction>125µm
0501.029[a]		604-607	605.5	3089	38	3209-3383	3296	Terrestrial botanical macrofossils
0501.029[a]		711-712	711.5	4129	42	4530-4821	4676	Terrestrial botanical macrofossils
0501.029[a]		1024-1029	1026.5	5790	40	6485-6676	6581	Terrestrial botanical macrofossils
0501.029[a]		1046-1050	1048	5900	45	6633-6805	6719	Terrestrial botanical macrofossils
64PE332-30-2		0-2	1				0	
64PE332-30-2	BETA 348791	20-22	21	500	30	40-236	138	Gastropod fragments
64PE332-30-2	BETA 348792	428-430	429	1730	30	1221-1349	1285	*Ammonia beccarii* (benthic forams)
64PE332-30-2	BETA 348793	678-680	679	2320	30	1848-2032	1940	Gastropod
64PE332-30-2	BETA 317911	976-978	977	5370	30	5643-5849	5746	Bivalve shell fragments
64PE332-44-2		0-2	1				0	
64PE332-44-2	BETA 317906	521-523	521.5	2330	30	1858-2044	1951	Mixed planktonic forams
64PE332-44-2	BETA 317907	770-772	771.5	5390	30	5664-5865	5765	Gastropod
64PE332-44-2	BETA 317908	924.5-926.5	925.5	8160	40	8515-8798	8657	Mixed planktonic forams
64PE269-39-4		0	0				0	
64PE269-39-4	BETA 330562	5	5	930	30	486-608	547	G. bulloides (planktonic forams)
64PE269-39-4	BETA 330563	100	100	4980	50	5205-5466	5336	G. bulloides (planktonic forams)
64PE269-39-4	BETA 330564	200	200	10190	40	11092-11271	11182	G. bulloides (planktonic forams)
64PE269-39-4	BETA 348794	280	280	11540	40	12865-13150	13008	G. bulloides (planktonic forams)

962 **Table 3.** Concentrations of GDGTs and brGDGT based indices for each sample set along the

963 transect.

Sample name	Age (cal. kyrs. BP)	TOC[a] (wt. %)	$\delta^{13}C_{TOC}$ [a] (‰ VPDB)	Concentration (μg gOC^{-1})		BIT index	MBT'_{5me}	DC'	IR	IR_{II}	IR_{III}
				Crenarchaeol	Sum brGDGTs						
Tagus soils											
TRS-8b	n/a	3.0	-27.8	2.2	19.2	0.88	0.51	0.13	0.39	0.36	0.43
TRS-7	n/a	5.0	-27.5	0.0	7.5	1.00	0.56	0.01	0.13	0.12	0.17
TRS-9	n/a	0.5	-27.2	0.1	7.8	0.99	0.68	0.01	0.14	0.14	0.15
TRS-3	n/a	0.7	-29.0	0.6	4.1	0.87	0.40	0.05	0.41	0.43	0.39
TRS-4	n/a	0.7	-28.7	1.2	5.3	0.81	0.42	0.04	0.39	0.41	0.30
TRS-5	n/a	2.2	-28.4	2.4	15.3	0.85	0.29	0.10	0.37	0.37	0.35
TRS-10	n/a	1.5	-28.5	1.4	1.6	0.49	0.60	0.19	0.84	0.88	0.83
TRS-12	n/a	0.2	-25.1	4.0	2.4	0.34	0.62	0.22	0.87	0.87	0.91
TRS-14b	n/a	0.8	-25.3	1.7	2.1	0.48	0.57	0.32	0.85	0.89	0.86
TRS-13	n/a	6.9	-27.0	0.9	1.2	0.54	0.33	0.13	0.74	0.80	0.71
TRS-15	n/a	0.9	-25.7	1.9	2.0	0.48	0.46	0.21	0.86	0.90	0.86
TRS-16	n/a	0.1	-24.8	1.6	3.0	0.62	0.56	0.19	0.92	0.93	0.93
TRS-20	n/a	0.1	-26.1	0.6	3.8	0.84	0.52	0.38	0.83	0.87	0.83
TRS-19	n/a	0.1	-25.7	0.7	19.7	0.95	0.56	0.44	0.84	0.85	0.89
Tagus Riverbank sediments											
TRS-6	n/a	1.7	-26.3	16.7	76.0	0.77	0.53	0.30	0.54	0.46	0.59
TRS-8a	n/a	0.2	-26.5	10.8	68.2	0.83	0.55	0.26	0.77	0.71	0.83
TRS 2a	n/a	3.3	-23.6	3.4	12.8	0.70	0.63	0.42	0.79	0.81	0.77
TRS 2b	n/a	0.5	-25.1	8.1	55.1	0.80	0.57	0.45	0.67	0.72	0.72
TRS 1a	n/a	0.9	-26.9	9.7	18.8	0.62	0.54	0.21	0.68	0.68	0.66
TRS1b	n/a	1.5	-27.6	26.1	19.7	0.28	0.64	0.53	0.72	0.82	0.80
TRS-11	n/a	1.3	-27.0	6.3	3.9	0.33	0.48	0.24	0.75	0.79	0.75
TRS-14a	n/a	3.0	-27.1	1.2	21.7	0.92	0.38	0.44	0.55	0.56	0.68
TRS-17	n/a	3.7	-29.6	1.6	37.8	0.93	0.41	0.51	0.70	0.65	0.66
TRS-22	n/a	0.6	-29.8	3.1	24.8	0.86	0.41	0.40	0.80	0.75	0.82
Tagus River SPM											
TR 2 Sup July	n/a	2.6	-29.2	6.2	33.1	0.80	0.51	0.28	0.60	0.53	0.64
TR 3#1 –Sup Sept.	n/a	1.8	-28.4	5.6	20.7	0.73	0.52	0.30	0.59	0.51	0.61
TR4 #1 Oct.	n/a	2.5	-30.9	8.6	38.1	0.77	0.52	0.30	0.61	0.54	0.62
TR5 #1 Sup Nov.	n/a	1.3	-28.9	5.8	54.8	0.85	0.49	0.25	0.62	0.55	0.68
TR 6 #1 Sup Dec.	n/a	2.4	-29.4	11.5	86.8	0.85	0.47	0.26	0.63	0.56	0.67
TR7 #1 Sup Jan.	n/a	2.4	-29.8	9.8	53.6	0.77	0.48	0.27	0.63	0.56	0.67
TR8 #1 Sup Feb.	n/a	1.0	-29.4	16.8	46.9	0.69	0.50	0.27	0.58	0.51	0.62
TR9 #1 Sup Mar.	n/a	2.2	-29.0	6.3	21.9	0.72	0.50	0.29	0.58	0.51	0.61
TR10 #1 Sup Apr.	n/a	1.9	-28.5	0.8	36.5	0.96	0.52	0.29	0.58	0.50	0.61
TR11 #1 Sup May	n/a	1.7	-28.5	26.3	80.8	0.69	0.52	0.29	0.56	0.48	0.59
TR12 #1 Sup June	n/a	1.3	-27.8	9.5	22.8	0.65	0.55	0.23	0.51	0.48	0.58

Tagus River Floodplain sediments (0501.029) depth (cm)											
10.0	0.0	1.7	-26.3	2.1	29.7	0.92	0.34	0.31	0.39	0.39	0.44
95.0	0.3	2.6	-26.5	6.4	66.8	0.89	0.36	0.24	0.43	0.43	0.45
195.0	0.6	1.5	-27.4	2.5	111.8	0.97	0.34	0.37	0.38	0.40	0.43
241.0	0.8	1.5	-26.0	5.2	62.0	0.90	0.40	0.24	0.35	0.36	0.38
341.5	1.0	11.2	-27.5	0.9	47.6	0.97	0.45	0.39	0.36	0.34	0.37
401.0	1.5	12.1	-27.7	1.2	90.6	0.98	0.38	0.38	0.40	0.36	0.46
453.0	2.0	8.0	-26.7	3.0	120.9	0.97	0.34	0.35	0.43	0.43	0.50
542.0	2.8	7.7	-27.3	3.2	91.9	0.95	0.37	0.39	0.40	0.41	0.42
577.0	3.1	4.6	-27.2	3.3	84.2	0.95	0.43	0.35	0.38	0.37	0.41
641.0	3.8	5.3	-28.1	1.0	59.6	0.97	0.52	0.39	0.34	0.35	0.39
681.0	4.3	6.6	-28.6	1.0	52.3	0.97	0.46	0.45	0.37	0.37	0.42
741.0	4.9	4.2	-24.4	4.2	74.3	0.92	0.43	0.45	0.38	0.38	0.36
862.0	5.6	16.2	-26.8	2.2	58.4	0.94	0.45	0.45	0.46	0.43	0.52
982.0	6.3	8.7	-27.7	1.5	46.5	0.95	0.46	0.49	0.37	0.36	0.37
1041.0	6.7	5.2	-27.2	4.4	48.2	0.87	0.48	0.45	0.40	0.39	0.41
Mudbelt sediments (64PE332-30-2) depth (cm)											
1.0	0.0	1.2	-23.7	200.9	28.5	0.09	0.58	0.35	0.51	0.45	0.54
25.0	0.2	1.0	-24.2	194.7	40.7	0.13	0.54	0.28	0.49	0.43	0.52
53.0	0.2	0.9	-24.5	189.3	36.4	0.13	0.52	0.26	0.47	0.44	0.50
75.0	0.3	1.0	-24.4	206.5	43.8	0.14	0.52	0.26	0.48	0.43	0.51
101.0	0.4	0.9	-24.3	228.9	44.4	0.13	0.53	0.27	0.48	0.43	0.51
151.0	0.5	0.9	-24.3	194.8	40.2	0.13	0.53	0.27	0.49	0.44	0.53
201.0	0.6	1.0	-24.5	187.9	31.9	0.11	0.51	0.27	0.47	0.43	0.50
248.0	0.8	0.6	-24.5	224.0	58.0	0.14	0.53	0.26	0.46	0.42	0.49
297.0	0.9	1.1	-24.5	168.3	30.6	0.12	0.50	0.26	0.47	0.42	0.51
347.0	1.1	1.0	-24.1	202.5	24.3	0.08	0.52	0.30	0.50	0.45	0.53
397.0	1.2	1.1	-24.1	180.4	27.3	0.10	0.49	0.30	0.48	0.43	0.52
429.0	1.3	1.2	-24.0	77.3	8.7	0.08	0.50	0.34	0.53	0.45	0.57
496.0	1.5	1.0	-24.3	143.8	15.1	0.07	0.52	0.32	0.53	0.46	0.57
546.0	1.6	0.9	-24.1	11.2	1.4	0.08	0.52	0.33	0.51	0.45	0.55
596.0	1.7	1.1	-27.3	141.3	14.8	0.07	0.51	0.34	0.52	0.45	0.56
645.0	1.9	1.1	-29.9	108.7	12.8	0.08	0.52	0.34	0.52	0.45	0.55
680.0	2.0	1.1	-27.4	142.1	17.4	0.08	0.54	0.31	0.50	0.44	0.54
741.0	2.7	0.8	-27.3	176.1	16.0	0.06	0.52	0.35	0.53	0.46	0.55
791.0	3.4	0.7	-24.5	240.8	19.8	0.05	0.50	0.37	0.55	0.48	0.58
840.0	4.0	0.9	-24.4	139.3	11.0	0.05	0.48	0.37	0.54	0.48	0.55
890.0	4.6	0.6	-24.6	180.2	14.2	0.05	0.48	0.39	0.55	0.47	0.57
977.0	5.7	0.7	-27.5	125.8	11.8	0.06	0.46	0.40	0.53	0.46	0.52
Lisbon Canyon Head sediments (64PE332-44-2) depth (cm)											
1.0	0.0	1.5	-22.9	420.5	27.1	0.04	0.60	0.41	0.55	0.48	0.56
45.0	0.2	1.2	-22.8	409.9	47.3	0.07	0.58	0.40	0.55	0.48	0.57

85.0	0.3	1.1	-23.4	440.4	48.1	0.07	0.54	0.36	0.53	0.46	0.55
130.5	0.5	1.2	-23.4	429.6	41.2	0.06	0.55	0.36	0.53	0.46	0.57
187.5	0.7	1.2	-23.7	308.4	27.6	0.06	0.56	0.36	0.53	0.45	0.56
221.5	0.8	1.1	-24.4	157.9	35.1	0.12	0.54	0.28	0.47	0.42	0.51
278.5	1.0	1.2	-23.2	283.6	22.7	0.05	0.54	0.36	0.51	0.45	0.54
326.5	1.2	1.0	-22.6	361.7	31.1	0.05	0.53	0.42	0.56	0.47	0.60
371.5	1.4	1.1	-22.6	374.1	26.5	0.05	0.53	0.41	0.55	0.47	0.58
429.0	1.6	1.0	-22.6	399.6	29.2	0.05	0.55	0.42	0.56	0.49	0.59
480.0	1.8	1.1	-23.4	242.3	18.0	0.05	0.54	0.41	0.55	0.48	0.57
502.0	1.9	1.1	-23.9	365.1	25.4	0.04	0.52	0.42	0.56	0.49	0.58
522.0	2.0	1.0	-23.4	376.8	30.9	0.05	0.55	0.39	0.55	0.48	0.57
550.0	2.4	1.0	-23.0	363.1	26.7	0.05	0.54	0.43	0.57	0.50	0.59
570.0	2.7	0.7	-22.6	493.6	34.3	0.04	0.53	0.43	0.57	0.50	0.59
630.0	3.6	0.7	-22.4	389.6	25.7	0.04	0.53	0.44	0.58	0.51	0.60
686.0	4.5	0.5	-22.4	640.2	40.7	0.04	0.54	0.45	0.59	0.51	0.60
728.0	5.1	0.5	-22.1	100.1	6.7	0.04	0.50	0.45	0.57	0.51	0.58
771.0	5.8	0.7	-23.3	620.7	37.3	0.04	0.53	0.44	0.58	0.50	0.59
805.0	6.4	0.3	-22.1	414.0	25.9	0.04	0.52	0.45	0.58	0.51	0.58
869.5	7.6	0.3	-22.3	538.9	35.7	0.04	0.54	0.41	0.57	0.50	0.56
925.5	8.7	0.3	-23.1	409.4	30.1	0.04	0.52	0.46	0.59	0.51	0.58
Lower Setúbal Canyon sediments (64PE269-39-4) depth (cm)											
1.0	0.0	0.8	-23.5	265.3	20.3	0.05	0.68	0.38	0.73	0.60	0.77
20.0	1.3	0.7	-22.3	506.5	15.6	0.02	0.60	0.39	0.77	0.60	0.80
40.0	2.3	0.6	-22.0	751.5	18.1	0.02	0.58	0.39	0.73	0.61	0.75
60.0	3.3	0.8	-22.2	540.7	16.2	0.02	0.56	0.46	0.75	0.61	0.74
80.0	4.3	0.8	-22.3	460.5	13.5	0.02	0.56	0.41	0.75	0.63	0.77
100.0	5.3	0.8	-22.8	204.7	7.3	0.03	0.57	0.37	0.74	0.66	0.75
120.0	6.5	0.7	-22.8	199.2	8.0	0.03	0.57	0.38	0.77	0.66	0.78
140.0	7.7	0.5	-26.1	433.3	13.6	0.02	0.51	0.41	0.73	0.67	0.74
160.0	8.8	0.5	-22.8	395.6	16.9	0.03	0.45	0.43	0.69	0.64	0.64
180.0	10.0	0.4	-24.9	709.2	25.6	0.02	0.48	0.43	0.69	0.58	0.65
200.0	11.2	0.5	-25.7	703.9	22.1	0.02	0.54	0.41	0.66	0.52	0.64
220.0	11.6	n/a	n/a	n/a	n/a	0.02	0.48	0.47	0.66	0.52	0.59
240.0	12.1	n/a	n/a	n/a	n/a	0.01	0.56	0.57	0.70	0.56	0.63
260.0	12.6	n/a	n/a	n/a	n/a	0.03	0.58	0.49	0.71	0.58	0.64
280.0	13.0	n/a	n/a	n/a	n/a	0.01	0.52	0.48	0.69	0.57	0.65

964 [a] Data for Tagus soils, riverbank sediments and SPM have previously been published by Zell et al. (2014).

Figure 1

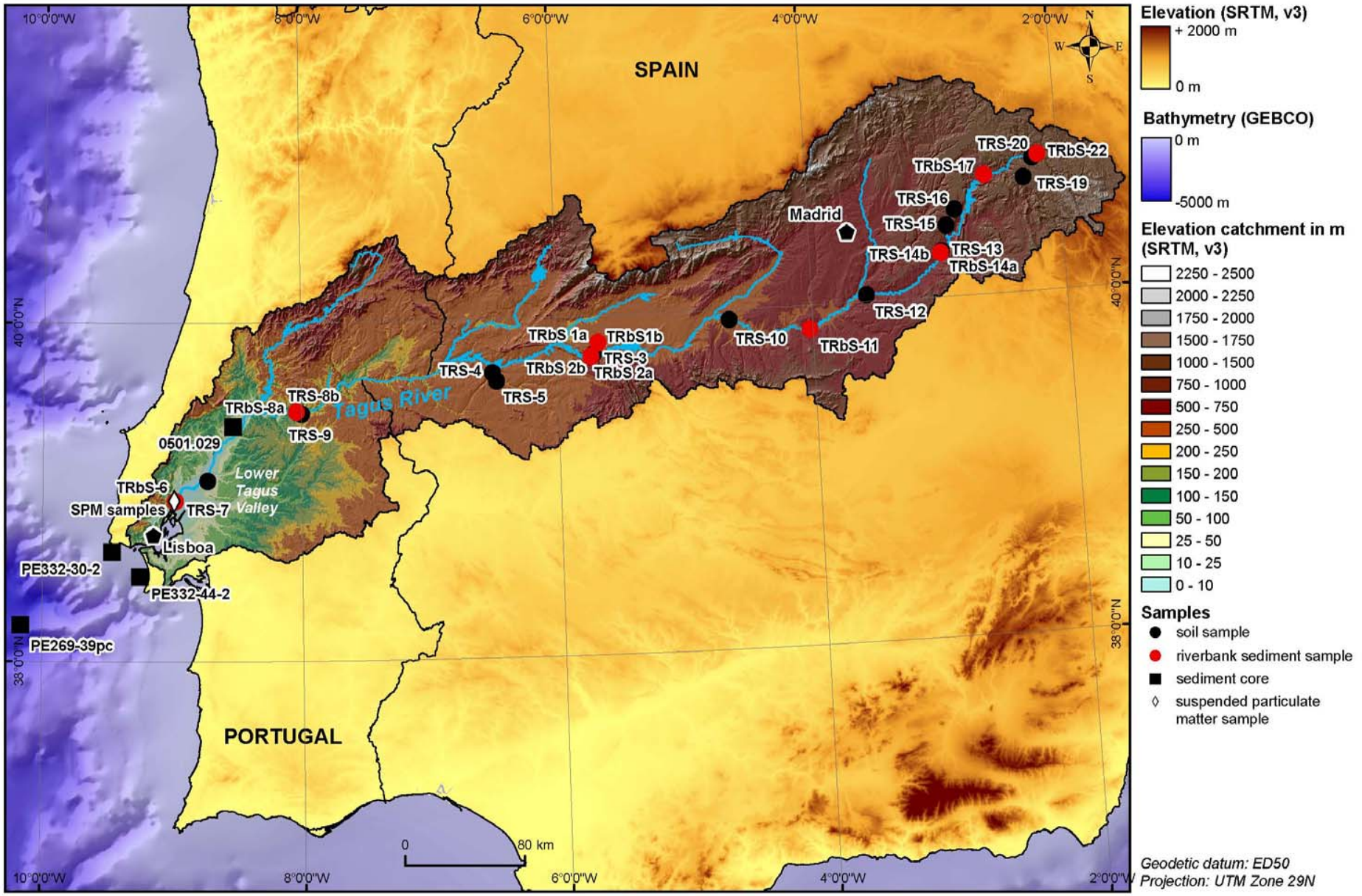
SPAIN
PORTUGAL
Madrid
Tagus River
Lower Tagus Valley
Lisboa
SPM samples
0501.029
TRS-20
TRbS-22
TRbS-17
TRS-19
TRS-16
TRS-15
TRS-14b
TRS-13
TRbS-14a
TRS-12
TRS-10
TRbS-11
TRbS 1a
TRbS1b
TRS-3
TRbS 2b
TRbS 2a
TRS-4
TRS-5
TRS-8b
TRbS-8a
TRS-9
TRbS-6
TRS-7
PE332-30-2
PE332-44-2
PE269-39pc
10°0'0"W
8°0'0"W
6°0'0"W
4°0'0"W
2°0'0"W
40°0'0"N
38°0'0"N
0
80 km
N
W
E
S
Elevation (SRTM, v3)
+ 2000 m
0 m
Bathymetry (GEBCO)
0 m
-5000 m
Elevation catchment in m (SRTM, v3)
2250 - 2500
2000 - 2250
1750 - 2000
1500 - 1750
1000 - 1500
750 - 1000
500 - 750
250 - 500
200 - 250
150 - 200
100 - 150
50 - 100
25 - 50
10 - 25
0 - 10
Samples
soil sample
riverbank sediment sample
sediment core
suspended particulate matter sample
Geodetic datum: ED50
Projection: UTM Zone 29N

Figure 2

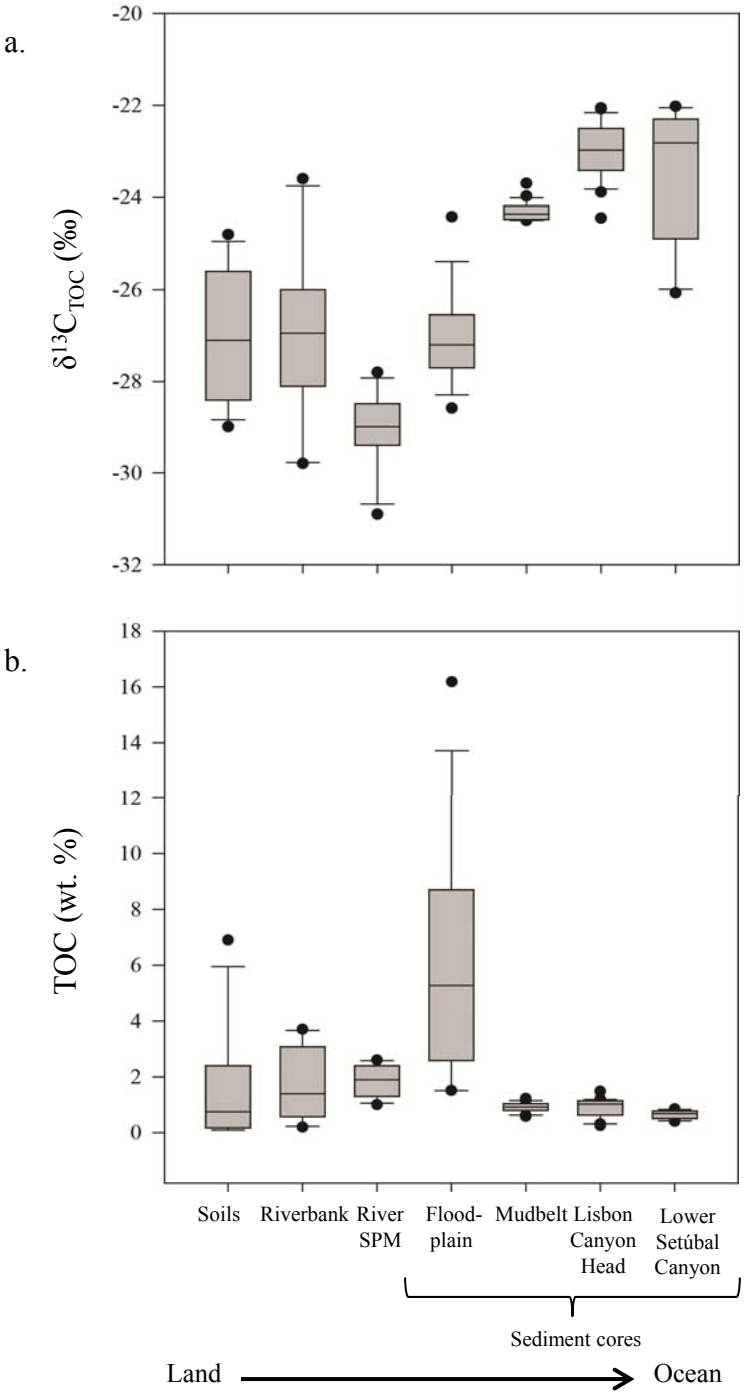
a.
-20
-22
-24
-26
-28
-30
-32
$\delta^{13}C_{TOC}$ (‰)
b.
18
16
14
12
10
8
6
4
2
0
TOC (wt. %)
Soils
Riverbank River SPM
Flood-plain
Mudbelt
Lisbon Canyon Head
Lower Setúbal Canyon
Sediment cores
Land
Ocean

Figure 3

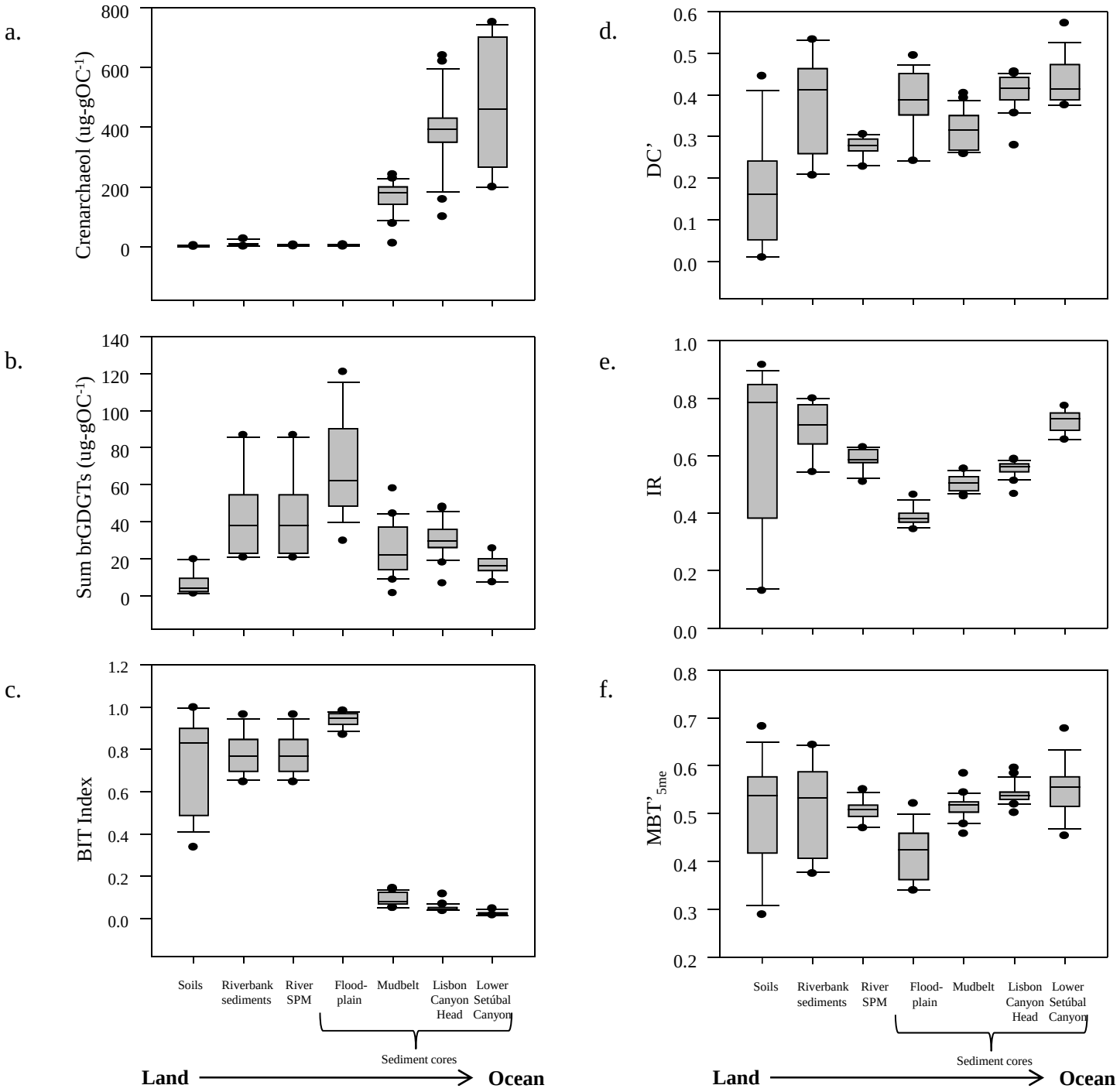
a.
Crenarchaeol (ug-gOC-1)
800
600
400
200
0
b.
Sum brGDGTs (ug-gOC-1)
140
120
100
80
60
40
20
0
c.
BIT Index
1.2
1.0
0.8
0.6
0.4
0.2
0.0
d.
DC'
0.6
0.5
0.4
0.3
0.2
0.1
0.0
e.
IR
1.0
0.8
0.6
0.4
0.2
0.0
f.
MBT'5me
0.8
0.7
0.6
0.5
0.4
0.3
0.2
Soils
Riverbank sediments
River SPM
Flood-plain
Mudbelt
Lisbon Canyon Head
Lower Setúbal Canyon
Sediment cores
Land
Ocean

Figure 4

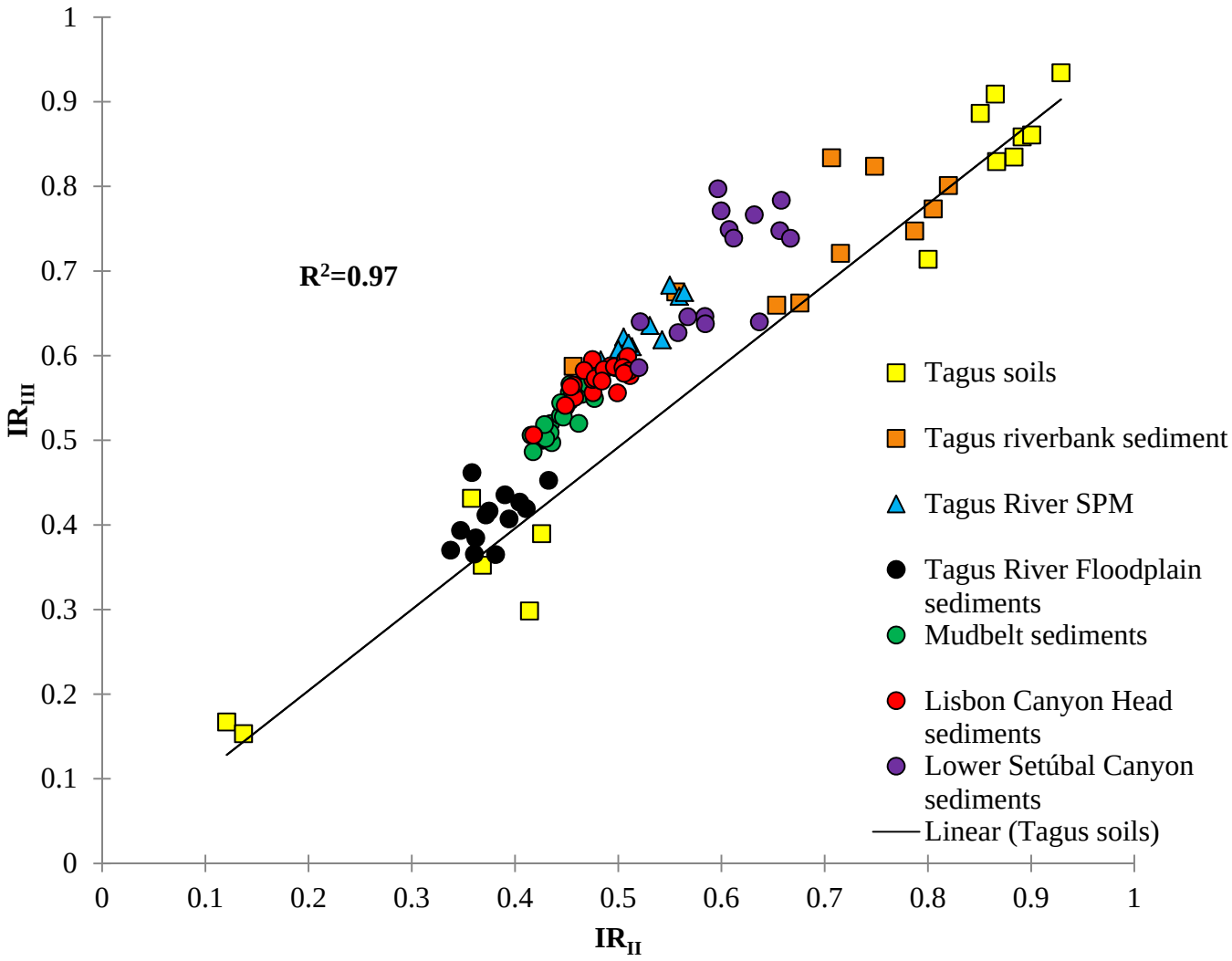
1
0.9
0.8
0.7
0.6
0.5
0.4
0.3
0.2
0.1
0
0
0.1
0.2
0.3
0.4
0.5
0.6
0.7
0.8
0.9
1
IRIII
IRII
R2=0.97
Tagus soils
Tagus riverbank sediment
Tagus River SPM
Tagus River Floodplain sediments
Mudbelt sediments
Lisbon Canyon Head sediments
Lower Setúbal Canyon sediments
Linear (Tagus soils)

Figure 5

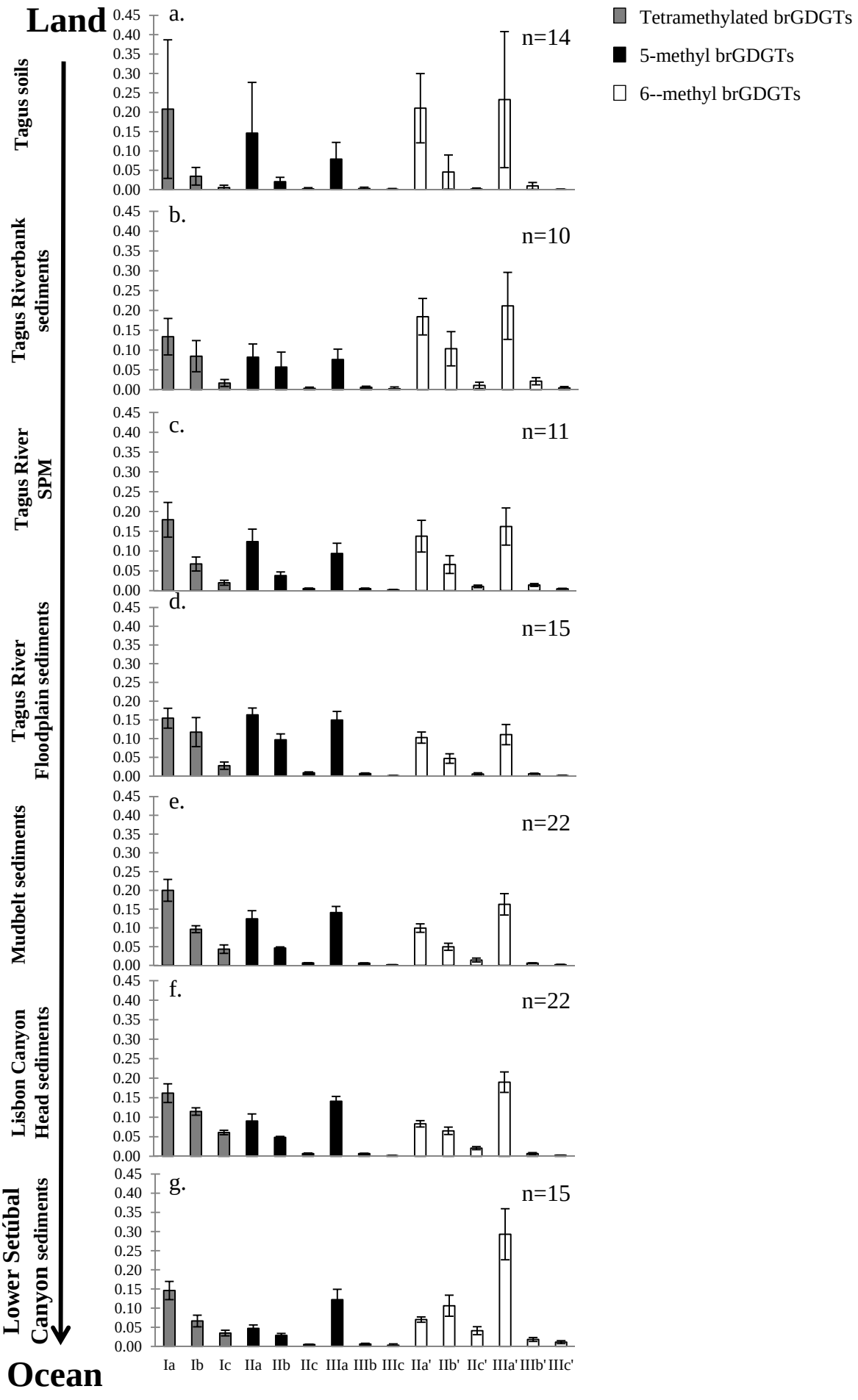
Land
Ocean
Tagus soils
Tagus Riverbank sediments
Tagus River SPM
Tagus River Floodplain sediments
Mudbelt sediments
Lisbon Canyon Head sediments
Lower Setúbal Canyon sediments
a.
b.
c.
d.
e.
f.
g.
n=14
n=10
n=11
n=15
n=22
n=22
n=15
Tetramethylated brGDGTs
5-methyl brGDGTs
6--methyl brGDGTs
Ia
Ib
Ic
IIa
IIb
IIc
IIIa
IIIb
IIIc
IIa'
IIb'
IIc'
IIIa'
IIIb'
IIIc'

Figure 6

a.

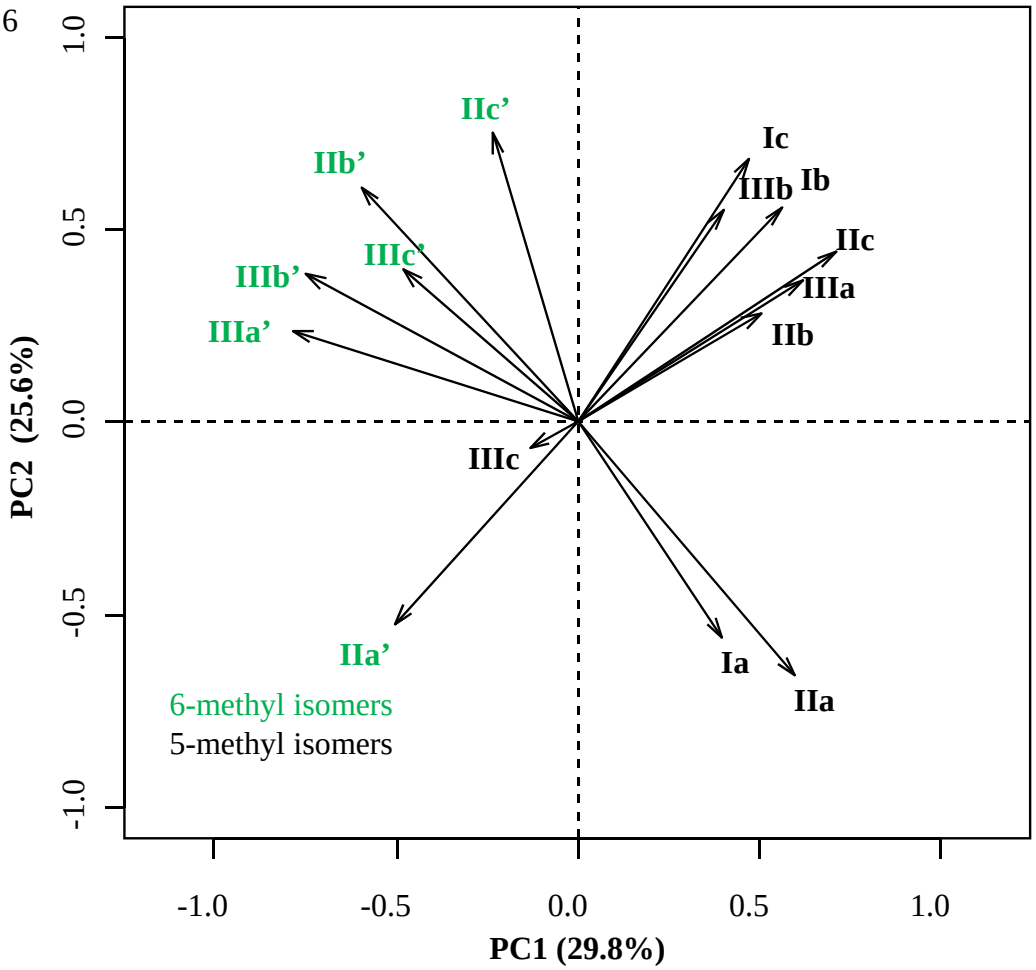
IIc'
IIb'
IIIc'
IIIb'
IIIa'
Ic
IIIb
Ib
IIc
IIIa
IIb
IIIc
IIa'
Ia
IIa
6-methyl isomers
5-methyl isomers
PC2 (25.6%)
PC1 (29.8%)
1.0
0.5
0.0
-0.5
-1.0

b.

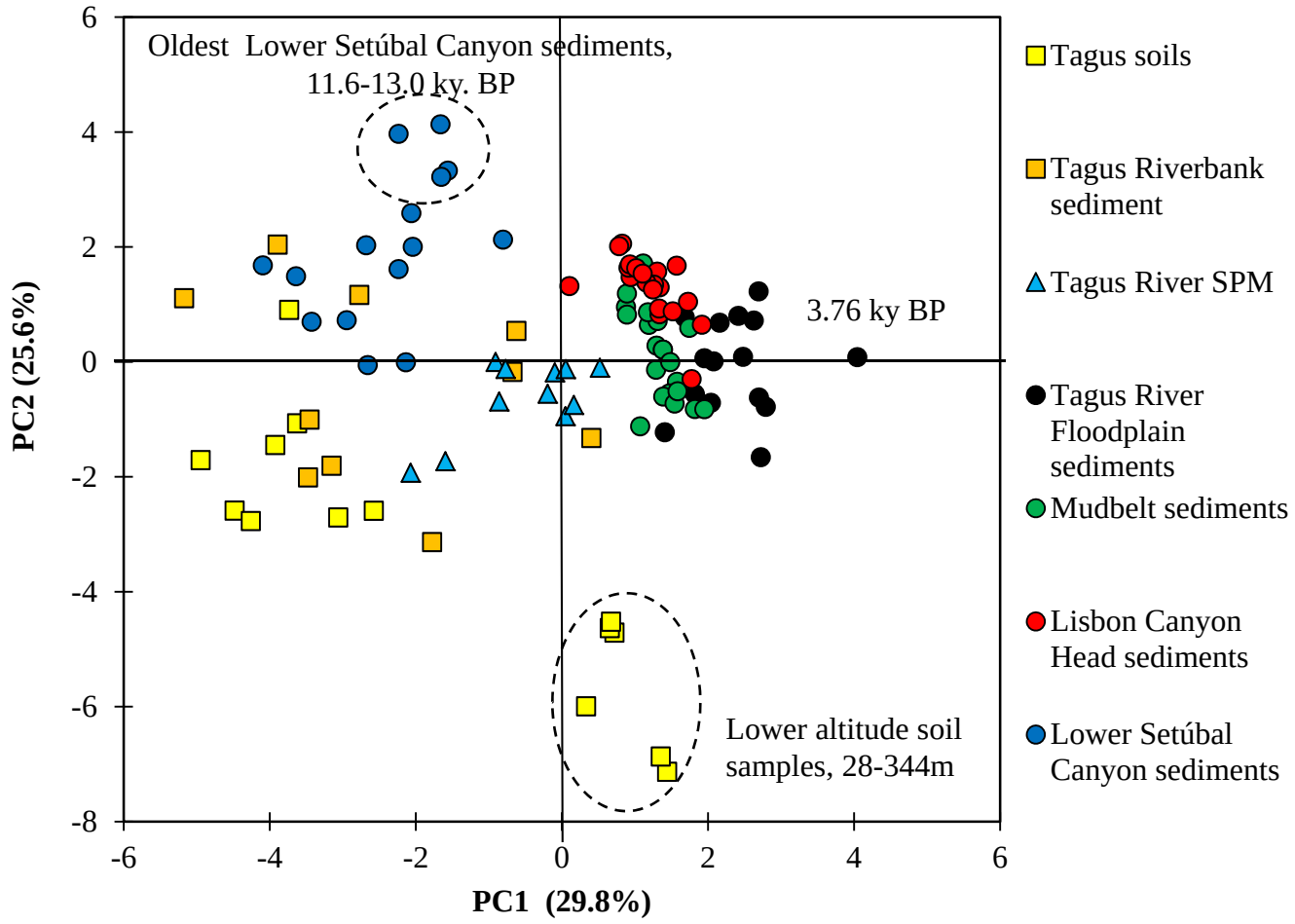
Oldest Lower Setúbal Canyon sediments,
11.6-13.0 ky. BP
3.76 ky BP
Lower altitude soil
samples, 28-344m
PC2 (25.6%)
PC1 (29.8%)
Tagus soils
Tagus Riverbank sediment
Tagus River SPM
Tagus River Floodplain sediments
Mudbelt sediments
Lisbon Canyon Head sediments
Lower Setúbal Canyon sediments

Fig. 7

a.

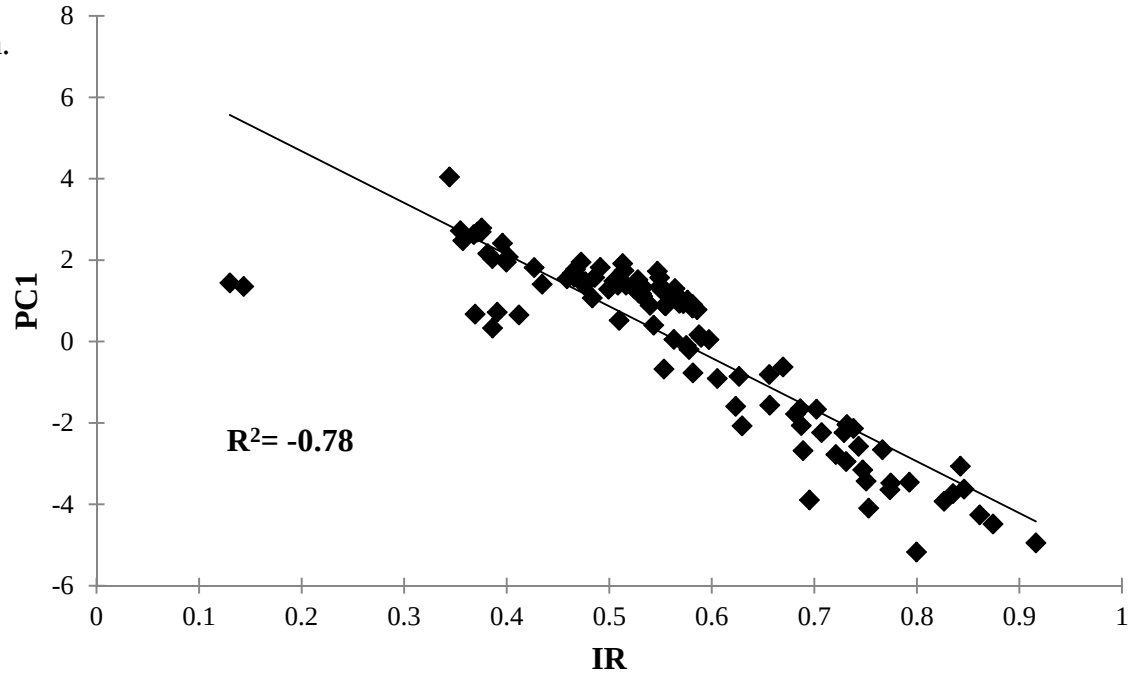
8
6
4
2
0
-2
-4
-6
PC1
R²= -0.78
0
0.1
0.2
0.3
0.4
0.5
0.6
0.7
0.8
0.9
1
IR

b.

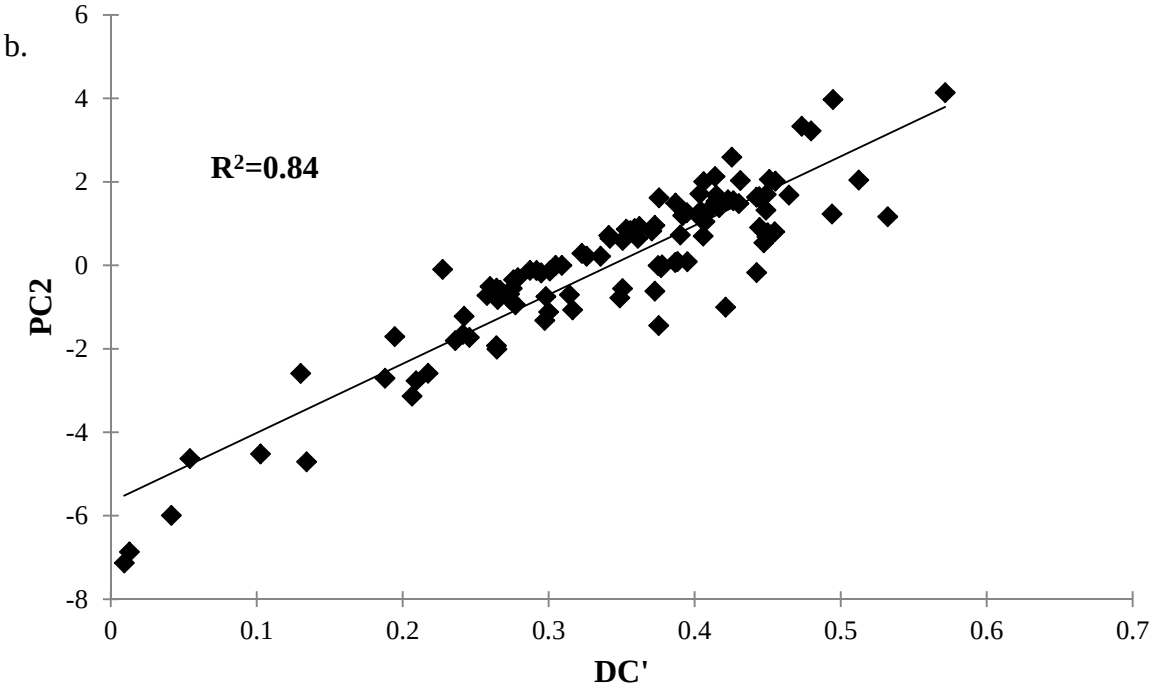
6
4
2
0
-2
-4
-6
-8
PC2
R²=0.84
0
0.1
0.2
0.3
0.4
0.5
0.6
0.7
DC'

Figure 8

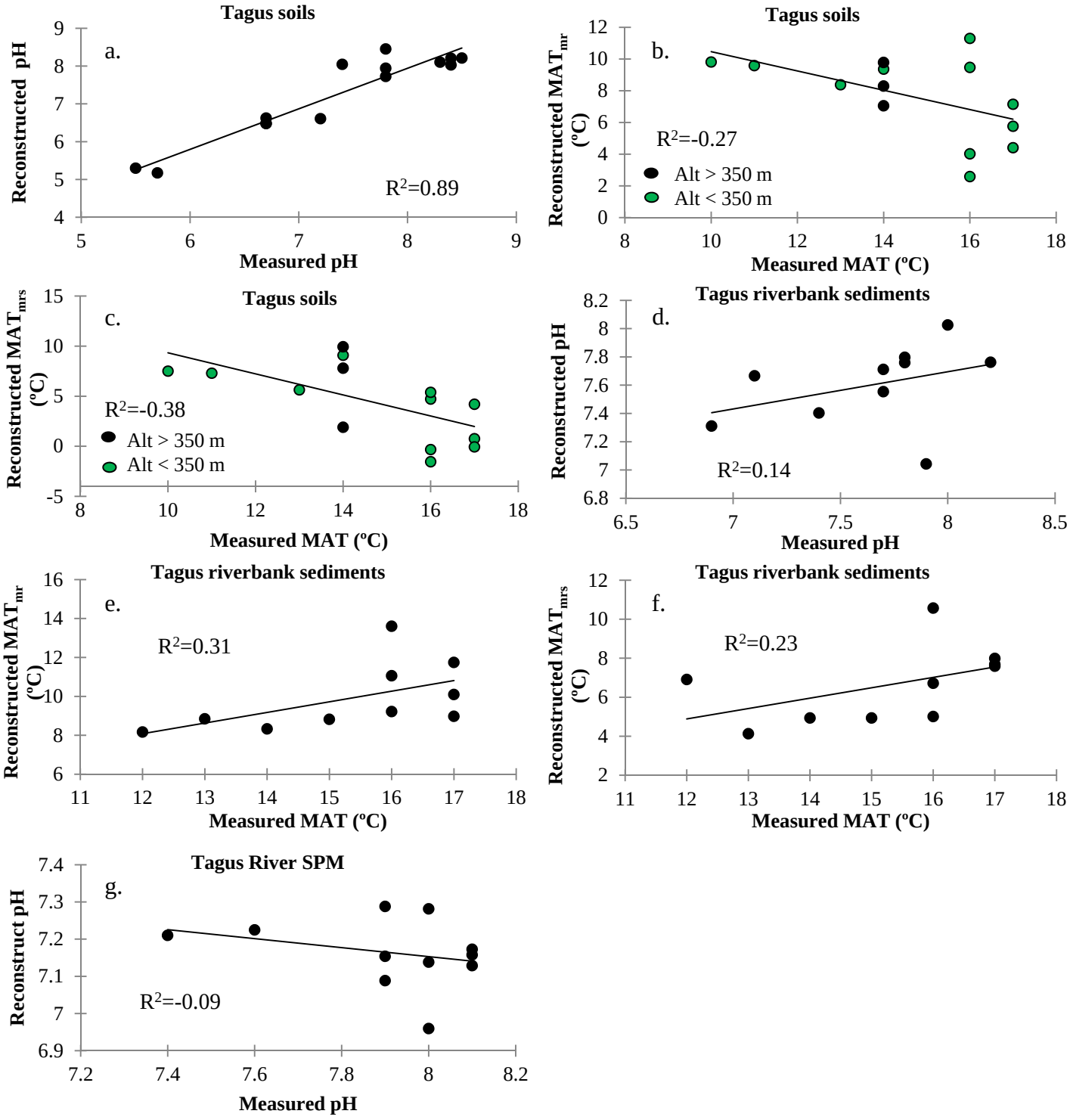
Tagus soils
a.
Reconstructed pH
Measured pH
R²=0.89
Tagus soils
b.
Reconstructed MAT$_{mr}$ (ºC)
Measured MAT (ºC)
R²=-0.27
Alt > 350 m
Alt < 350 m
Tagus soils
c.
Reconstructed MAT$_{mrs}$ (ºC)
Measured MAT (ºC)
R²=-0.38
Alt > 350 m
Alt < 350 m
Tagus riverbank sediments
d.
Reconstructed pH
Measured pH
R²=0.14
Tagus riverbank sediments
e.
Reconstructed MAT$_{mr}$ (ºC)
Measured MAT (ºC)
R²=0.31
Tagus riverbank sediments
f.
Reconstructed MAT$_{mrs}$ (ºC)
Measured MAT (ºC)
R²=0.23
Tagus River SPM
g.
Reconstruct pH
Measured pH
R²=-0.09

Figure 9

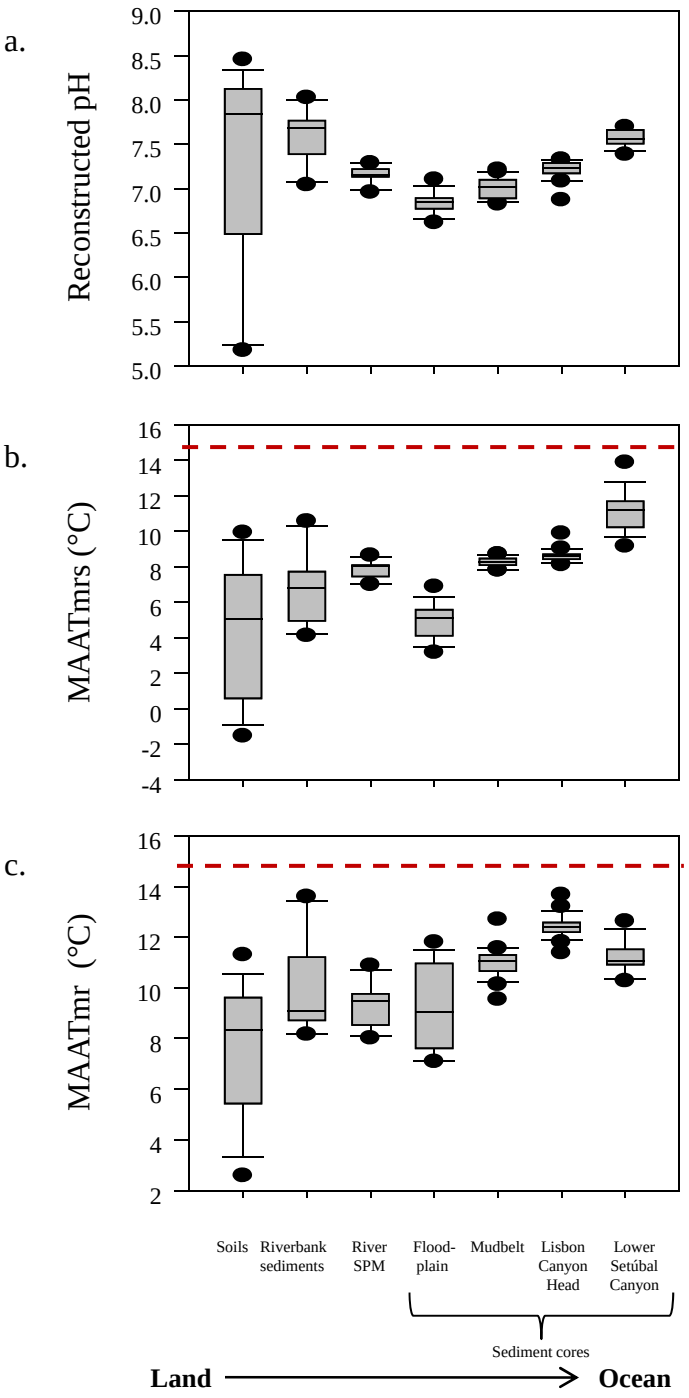
a.
Reconstructed pH
9.0
8.5
8.0
7.5
7.0
6.5
6.0
5.5
5.0
b.
MAATmrs (°C)
16
14
12
10
8
6
4
2
0
-2
-4
c.
MAATmr (°C)
16
14
12
10
8
6
4
2
Soils
Riverbank sediments
River SPM
Flood-plain
Mudbelt
Lisbon Canyon Head
Lower Setúbal Canyon
Sediment cores
Land
Ocean